

## Author's response

### Reviewer#1 – Virginie Pinel

#### 1. Main points

1) I enjoyed reading the introduction because the topic addressed is very important and this point is pretty well explained. But then I was somehow disappointed by the study itself. It is intended to evaluate the influence of geological data integrated into the modeling but only the stratigraphy and geometry of the plumbing system (see section 4) is considered. There is no real novelty in considering these aspects, which has been done in several studies (e.g. Cianetti et al, GJInt, 2012). I was expecting the authors to also take into consideration the existing faults after the long description of the structural/tectonic context of Colima volcano (fig1, section 2.1). In particular, the profile chosen for modeling cuts 2 faults of the Colima Rift, which are not considered in the models. Only a uniform extension applied at the lateral boundary is considered in some models. However, there are ways to consider a fault plane in 2D using a friction law (see Chaput et al, GRL 2014).

*We thank the reviewer for the useful comments. The manuscript has been submitted for the special issue on the use of geological data for constraining numerical models. We focused our attention to geology (stratigraphic data, geometry of the feeding system) of the Colima Volcano area. However, we are aware the approach is not new, but it is new for Colima volcano. Moreover, it provides further insights on the limitations of FEM analysis when some geological features are unknown or not considered. The insertion of a constant extensive stress is not trivial, because it simulates the stress state that dominates the Colima rift over long times, affecting the computational domain. However, we agree that the fault movement (and the fault plane itself) may induce different perturbation in the stress state of the conduit feeding system area. However, although LISA cannot include a frictional law as in Chaput et al. (2014) and cannot provide the solution for two separated domains at the same time, in order to consider Reviewer#1's criticism, in the revised version we considered an approximate description of the effects of faults. In particular, since mature fault zones are generally made of complex highly deformed and low cohesive materials where most of the fault displacement is accommodated and surrounded by a fractured damage zone, in this revised version of the manuscript we have provided a new final configuration considering the faults of the Colima graben as "damage zones". Technically, we have selected two bands of elements by assigning more degraded elastic properties (as reported in Jeanne et al. 2017). Results with considering the fault are provided in the new Figure 7.*

2) Model assumptions are not clearly described.

- It is in 2D but it is not explained whether a plane strain or a plane stress approximation is considered, which is a key information. Usually models are performed in plane strain, which means that there is a stress component out of plane.

*We thank the Reviewer for such a point. Now we clearly stated that it is a plane strain in the text.*

-The way the gravitational loading is applied remains unclear. When applying body forces lithostatic stress field should also be applied but when a topography is considered, some iterations

are required to find the initial state of stress consistent with both the topography, the rheology and the body forces as described in Chaput et al, GRL, 2014 or Cianetti et al, GJI, 2012. Also with a lithostatic stress field, the load applied at the reservoir boundaries has to be a superposition of the overpressure and the lithostatic component. It is not explained in the manuscript. Also if a lithostatic stress field is applied both the minimum and maximum stress field should increase with depth. From the figures shown in the result section it is not the case for the minimum stress  $\sigma_3$  and I don't really understand why.

*We described better this point in the text. The load applied to magma chambers is exactly the same requested by the reviewer (a superposition of the magmatic overpressure and the lithostatic component). Both  $\sigma_1$  and  $\sigma_3$  increase with depth, as shown in Figure 4 where it can be seen  $\sigma_3$  passes from zero to 110 MPa at depth.  $\sigma_1$  passes from zero to ca 390 MPa. Probably, the reviewer was erroneously confused by the same colour scale applied to both Figures. In order to avoid confusion we clearly highlighted this point about colour scale in the revised text.*

3) Illustrations should be improved to help the understanding. In some cases, the dimensions of the numerical box represented are not clearly reported, titles are unclear. I will detail later on each figure. *Figures have been improved in this revised version.*

## 2. Minor points

1) Regarding the results and discussion of the Young modulus influence on the stress field, what matters are the ratios of the Young modulus considered in various layers and not the absolute value of the Young modulus in one given layer (I mean that if the Young modulus is multiplied by 10 in each layer, no changes are expected except in the vicinity of the domain external boundaries). This fact is not clearly shown. Also I would recommend to cite the paper by Heap et al. published recently in the Journal of Volcanology and Geothermal Research (<https://doi.org/10.1016/j.jvolgeores.2019.106684>).

*In the light of what reported in Heap et al. (2020) about the selection of the most appropriate Young's Modulus in modelling, we would like to point out that in our parametric study we aimed to show what influence has the choice of different values of Young's Modulus in each geological unit at changing different feeding system configurations (i.e. single chamber, double chambers not connected and connected with conduits). The results demonstrated that the changes are not only in the vicinity of the external boundaries as expected, but also (even small) around the shallow magma chamber and conduits.*

2) Introduction: line 37, 41, before the chosen references list for numerical models I would put "e.g." because there are plenty of references that could be equally fairly cited here. Also I would add the reference to Cayol & Cornet, GRL, which is really a classical one. Line 57, I would suggest to also cite Albino et al., Geophysical journal international, 2010. *Added.*

3) Section 3.3 Line 213: it would be very helpful to show the mesh used. *Added in Figure 1 (panel c);* line 217, the boundary condition applied on the reservoir and dike walls should be explained. *We explained in the text.*

Line 229, the way gravity is expected to influence the failure condition is really depend on the rupture criterion considered (see for instance Albino, et al. JGR, 2018). *We specified this adding the suggested reference.*

Line 231, in Corbi et al, 2015, the trajectory of magma propagation is not influenced by gravity but by the deviatoric stress field induced by caldera unloading. *Thanks for such a comment. We corrected it in the text removing the reference.*

4) Section 4.2: Line 296 “During ascent to the surface, the dykes align themselves with the most energy-efficient orientation, which is roughly perpendicular to the least compressive principal stress axis  $\sigma_3$  (e.g. Gonnermann and Taisne, 2015; Rivalta et al., 2019).” this is true providing the magma driving pressure remains small compared to the deviatoric stress (see Pinel et al, JGR, 2017 and Maccaferri et al. G3, 2019). *We specified this in the text, also adding the suggested references.*

5) Section 5.1 Line 345, it would be important to show on a figure the reduced simulation domain selected for the sensibility analysis. Also for each unit, we would need to know the number of nodes considered (size of the vector space X). It is important because the larger variability of Unit B could be only due to the larger domain considered.

*We added the number of nodes for each geological Unit, in Table 1 (beside the number of elements).*

6) Figure 2: Figures labels and title should be improved, information of the number of nodes considered should be added. *We added the requested information in the captions.*

7) Figure 3: Figures labels and title should be improved, information of the number of node considered should be added. Limits of the different units should be shown. For panel A, it remains unclear to me which stress perturbation is considered as there is no reservoir.

*We improved the labels of Figures 2-3 adding the requested information. We preferred to not indicate the limits of the different units because they would not be clear with this scale. For the panel (a) of Figure 3, the stress perturbation is only due to the lithostatic load.*

8) Figure 5: The topography doesn't look the same on each panel, which makes comparison difficult. No indication is provided on the orientation of the maximum and minimum compressive stress. I don't understand the term "distensive". Once again I don't understand why  $\sigma_3$  does not increase with depth.

*Topography was corrected. The term “distensive” was changed into “extension”. We do not understand to what refers the reviewer when talking about orientation of maximum and minimum compressive stress. We already replied earlier about the increase of  $\sigma_3$  with depth.*

## **Reviewer#2 – Adelina Geyer**

### 1) General points

1) When citing previous published works use “e.g.” because the lists are not exhaustive and the

cited articles are just a small example of the existing references. *We added “e.g.” in the lists where citations are not exhaustive.*

2) The introduction is a bit confusing to me because the title (and objectives) of the manuscript are focused on stress field and the first paragraph of the introduction is about volcano deformation. I would recommend the authors to rethink the introduction pointing out the importance of calculating the stress field in volcanic areas, which are the components of the stress field (i.e. those processes affecting/modifying it, etc). Then, they can connect all this with the FEM as a “numerical tool” to quantify/predict the stress field in a volcanic area.

*We agree to point out the issue of calculating the stress field in the volcanic areas within the introduction. We added this part in the Introduction.*

3) The objectives of the work are presented in two different parts of the introduction (L68-74 and 83-86). I suggest merging them at the end of the introduction. *We merged the sentences at the end of the Introduction.*

4) To better evaluate the influence of the diverse geological details on the results obtained, it would be more appropriate to carry out first a parametric study on the studied parameters (e.g., Young’s modulus, Poisson ratio, magma chamber geometry). Keeping all parameters constant and changing one parameter at a time in a systematic way, is what really allows estimating (and quantifying) the influence of the individual parameters on the numerical results obtained (see, for example, Kinvig et al. 2009; Geyer & Gottsmann 2010). Once the parametric study has been done, results obtained can be applied to the case studies.

*The parametric study was carried out on Young’s modulus but may be easily carried out for Poisson’s ratio. In any case, the investigation of different parameters (i.e. rock mechanics and magma chamber geometry) would result in increasing the length of the paper, which is instead focused on influence of geological data (i.e. stratigraphy of the domain, feeding system geometry, effect of the rifting) on FEM simulations. However, we cited the papers mentioned by the reviewer in order to highlight the importance of the rock mechanics parameters.*

5) The authors should be sure that all names mentioned in the text are included in the figures. For example, Figure 1 showing the geological setting of the CVC does not show the location of the Michoacan Block, the Chapala-Tula rift, etc.

*We changed the citation in the text considering what reported in Norini et al. (2010-Figure 1) in which all mentioned geological structures are represented.*

6) It would really help to include a sketch of the CVC plumbing system. *We added it in the new version of Figure 1 (panel d).*

7) The authors should show the mesh and also provide details about the size of the elements, not only the number. *We included the mesh used in our modelling in Fig. 1 – panel (c), and we provided more information in the text about the mesh elements of each geological unit.*

8) The authors should better describe how gravity is implemented and how is the resultant stress

field derived from it considering the selected mechanical properties of the computational domain. Also, since there is topography, I do not understand what the authors mean with “Gravity in the host rock ( $z \leq 0$ )”. Is gravity not assigned for  $z$  values  $> 0$ ? This part should be clearly explained because the “background stress field” generated by the gravitational loading may have a strong influence on the results obtained.

*We provided a better explanation in the text. We also removed “( $z \leq 0$ )”.*

9) Considering the size and depth of the deep magma chamber, I think that the domain boundaries are far too close to the area of study, specially to the W. This is also acknowledged by the authors (L382-389). Considering that the models are 2D (i.e. computational time is not too high compared to 3D models), it would have been safer to expand the limits of the computational domain further away from the magma reservoirs. The “displacement = 0 m” boundary condition has strong effects on the results obtained if the boundary is too close to the pressure source.

*We showed the boundary effect in Figure 4. It is evident how the area comprising the feeding system (visible in Figs. 5-6-7) is not affected by any false result. To enlarge the domain would result in degrading of the details of the FEM simulation, which are already biased by the huge area at present considered for simulations.*

10) L49-51: I do not understand this sentence. What do the authors mean by “boundary representation”? Please, be sure that you are not confusing the Boundary Element Method (BEM) with the Finite Element Method (FEM).

*We revised the paragraph in the text in order to not be confusing. In particular, beside FEM, we aimed to describe another common way to describe the geological units by using BEM.*

11) L55-58: I would mention also the use of FEM for fluid dynamics or thermal problems to illustrate their application to solve other type of physical equations, not only those related to rock mechanics (e.g., Bea 2010; Gutiérrez & Parada 2010; Gelman et al. 2013; Douglas et al. 2016).  
*Done.*

12) L59-60: Use “e.g.” *Done.*

13) L60-62: Add references and indicate in GPa what is meant by “stiff” and “low”. *Done.*

14) L67-69: Include some references to illustrate what kind of publications already exist. *Done.*

15) L74: I think something is missing in this sentence.

16) L81-83: Please, revise this sentence. I think that something is not correct in the English, a native English speaker should verify it. *Corrected in the text.*

17) L87-92: What overpressure? This sentence is confusing. All this paragraph should come much earlier in the introduction, when presenting the problematic the authors want to solve. If the idea is to highlight the limitations of the elastic approach used in the models, this section should be move to the “Methodology” section. *We specified: ”estimate of magmatic overpressure”.*

18) L95: The CVC acronym has been already explained. L112: Where is all this information shown in Figure 1? L130: “a.s.l.” L186-188: What do the authors mean with “complex” structure? L193: Extension or extent?

*Corrections made in the text. We changed the citation from Figure 1 to Norini et al. 2010 – Fig 1). For “complex structure” we referred to the dual magma chamber system.*

19) L198: Indicate the website and what INEGI means. *Done.*

20) L215: Which geological units? The magma chamber? The rock layers? This sentence is confusing. *We referred to the extent of the rock layers, described in the following text and detailed in Table 2.*

21) L222-224: Since the authors have already extensively described it in the previous section maybe they should refer to their own text (and figure) here.

*In the previous section (3.3 Modelling approach) we referred to Spica et al. 2017 but other parameters used in our modeling are described in other papers (i.e., Massaro et al. 2018, 2019) therefore we think it is useful add here these citations. We also added the reference to Figure 1d.*

22) L224-227: Not sure which is the objective of this sentence, as the authors do not explain the overpressure assigned to their models in this paragraph. Is something missing? *No, in this sentence we only reported a general statement.*

23) L228: Commas are missing after between and with, otherwise the sentence is difficult to understand. *Done.*

24) L258: Please, add references. L260-261: Please, add references. Figures: Figure 1: Indicate the north arrow in (a). *Done for references. Figure 1: the North is on the top, left-side corner.*

25) Figure 4: The color different between Unit VD and GF is practically undistinguishable. It seems that the top-left image has a different orientation than the others. The selected color scale is strongly conditioned by the boundary effects at the right and left corners at the free surface. The authors should recalibrate the color scale so that the gravity stress field is visible also at shallower depths. Now is all in green.

*We changed the colour of Unit GF. About the colour scales, they were set in a way they represent all the four panels, in order to facilitate comparison. We are aware of the similarity of green colors, and for this we separated the different colours with dashed line to indicate changes in the stress value.*

26) Figure 5: It is really confusing to have to color scales for (a) and (b). It is difficult to compare the results between both models and the effect of the shallow reservoir. Has model b the gravitational loading implemented? It is strange to me to see that model provides negative sigma 1 values at such depths (i.e. 15 km).

*The different colour scales were used, in this case, just for avoiding the problem highlighted in the*

*previous point by the reviewer. To have a common scale would result in too large stress classes (with the same colour) that would prevent the readability of each example. Both models have the gravitational loading implemented. You have to bear in mind that changing geological conditions results in changes in while stress in the simulation, which prevents the use of a common colour scale in LISA. The moderate negative  $\sigma_1$  values are due to the effects of magma chamber overpressure with respect to the lithostatic load.*

27) Figure 6: I strongly recommend using another color scale, similar to the one in Figure 5 going from red to blue colors. In the sigma 1 picture many details are lost because of it.

*It is not possible to freely set the colour scale in LISA. The alternative colour scales provided by LISA are grey-scale and red-blue but they do not provide a better visualization than this shown in Figures (rainbow colour scale). Unfortunately, the details of  $\sigma_1$  are lost also in this case.*

28) Figure 7: Same comment as in Figure 5. Is in the model in the middle gravity implemented? To facilitate the comparison among all pictures, the same color scale for all sigma 1 and for all sigma 3 should be assigned. Otherwise is very confusing because the same colors are sometimes  $<0$  and other times  $>0$ .

*Also in this case the gravitational loading has been implemented. As already stated before, the addition of different geological details changes the stress distribution and its value. For this, it is not possible to use the same colour scale for all the simulations, otherwise we would have very broad, poorly informative scale of stress values.*

On behalf of the authors  
Sincerely,

*Silvia Massaro*

# **Analysing stress field conditions of the Colima Volcanic Complex (Mexico) by integrating FEM simulations and geological data**

Silvia Massaro<sup>1,2</sup>, Roberto Sulpizio<sup>1,2,3</sup>, Gianluca Norini<sup>2</sup>, Gianluca Groppelli<sup>2</sup>, Antonio Costa<sup>1</sup>,  
Lucia Capra<sup>4</sup>, Giacomo Lo Zupone<sup>5</sup>, Michele Porfido,<sup>6</sup> Andrea Gabrieli<sup>7</sup>

<sup>1</sup>Istituto Nazionale di Geofisica e Vulcanologia, Via D. Creti 12, 40128, Bologna, Italy.

<sup>2</sup>Istituto di Geologia Ambientale e Geoingegneria, Consiglio Nazionale delle Ricerche, Via M. Bianco 9, 20131, Milan, Italy.

<sup>3</sup>Dipartimento di Scienze della Terra e Geoambientali, Via E. Orabona 4, 70125, Bari, Italy.

<sup>4</sup>Centro de Geociencias, Universidad Nacional Autonoma de Mexico, Queretaro, Mexico.

<sup>5</sup>Institute of New Energy and Low-carbon Technology, Sichuan University, Chengdu, PRC.

<sup>6</sup>Alumni Mathematica, Dipartimento di Matematica, Via E. Orabona 4, 70125, Bari, Italy.

<sup>7</sup>Hawai'i Institute of Geophysics and Planetology, 1680 E-W Road, Honolulu, Hawai'i 96922, USA.

\*corresponding author: Silvia Massaro ([silvia.massaro@ingv.it](mailto:silvia.massaro@ingv.it))

## **Abstract**

In the last decades numerical methods have become very popular tools in volcanological studies, since capable of considering many relevant parameters in their calculations, such as the presence of multiple reservoirs, topography, and heterogeneous distribution of host rock mechanical properties. Although the widespread availability of geodetic data is keep growing, the influence of geological data on the numerical simulations is still poorly considered. In this work a 2D Finite Element Modelling is provided by using the **L**inear Static Analysis (LISA) software, in order to investigate the stress field conditions occurring around the Colima Volcanic Complex (CVC, Mexico) at increasing the details of geological and geophysical input data. By integrating the published geophysical, volcanological, and petrological data, we provide a first-order **description of the** domain of the CVC feeding system, considering either one or two magma chambers connected to the surface via dykes or isolated (not connected) in the elastic host rocks. We test the methodology by using a gravitational modelling with different geometrical configurations and constraints (i.e. magma chamber dimensions, depth, overpressure). Our results suggest that an appropriate set of geological data is of pivotal importance for improving the mesh generation procedures and the degree of accuracy of numerical outputs, aimed to more reliable physics-based representations of the natural systems.

## **1 Introduction**

Magmatism and tectonism in volcanic active areas are strongly related to the regional and local stress fields, affecting both the orientation of faults and the location of volcanic vents, two fundamental



38 [aspects when interpreting volcanic unrest and forecasting volcanic eruptions \(Geyer et al., 2016\). The](#)  
39 [stress field around a magmatic source originates from three main contributions: \(1\) the background](#)  
40 [stress, composed of a vertical gravitational load and a lateral horizontal load corresponding to](#)  
41 [lithostatic confinement and tectonic regimes; \(2\) the stress field caused by the loading of the volcano](#)  
42 [edifice; and \(3\) the stress field generated by the magmatic overpressure in the chamber system \(e.g.](#)  
43 [Martí and Geyer, 2009; Currenti and Williams et al., 2014\). In recent years, a large number of semi-](#)  
44 [analytical and numerical solutions for the stress field state of geological and volcanological systems](#)  
45 [have been proposed \(e.g. Cayol and Cornet, 1998; Simms and Garven, 2004; Manconi et al., 2007;](#)  
46 [Long and Grosfils, 2009; Currenti et al., 2010; Currenti and Williams et al., 2014; Zehner et al.,](#)  
47 [2015\), taking into account the static elastic deformation in a multi-layered half-space \(e.g. Dieterich](#)  
48 [and Decker, 1975; Bonafede et al., 2002; Wang et al., 2003; Gudmundsson and Brenner, 2004; Zhao](#)  
49 [et al., 2004; Pritchard and Simons, 2004; Gottsmann et al., 2006; Geyer and Gottsmann, 2010; Zhong](#)  
50 [et al., 2019\). Following the successful application in mechanical engineering, the use of Finite](#)  
51 [Element Method \(FEM\) has been extensively introduced in Earth Sciences in order to investigate the](#)  
52 [effects of topography, lithologic heterogeneities, tectonic stresses and the gravity field on the Earth's](#)  
53 [surface deformation \(e.g. Cailleau et al., 2003; 2005; Buchmann and Conolly 2007; Manconi et al.,](#)  
54 [2009; Masterlak et al., 2012\), including volcanoes \(e.g. Fujita et al., 2013; Carcho and Gàlan del](#)  
55 [Sastre, 2014; Bunney, 2014; Ronchin et al., 2015; Hickey et al., 2015; Cabaniss et al., 2019; Rivalta](#)  
56 [et al., 2019\).](#)

57 The use of FEM in volcanic areas has several examples, which vary from the influence of layered  
58 materials on the surface deformation process during volcanic inflation (e.g. Darwin volcano,  
59 Galapagos Islands; Manconi et al., 2007; [Albino et al., 2010](#)) to processes affecting chamber rupture  
60 (e.g. Grosfils, 2007; Long and Grosfils, 2009). [FEM is also used in fluid dynamics and](#)  
61 [thermodynamics \(e.g., Gutiérrez and Parada, 2010; Gelman et al., 2013\) for solving issues related to](#)  
62 [motion of fluids and heat transfer.](#)

63 The local stress around a volcanic feeding system strongly depends on the magma chamber geometry  
64 and on the mechanical properties of the layered host rock around it (e.g. Martí and Geyer, 2009),  
65 [mainly due to broad changes in Young's modulus \(e.g. Gudmundsson et al., 2011; Jeanne et al.,](#)  
66 [2017; Heap et al., 2020\).](#) For instance, limestones, lava flows, welded pyroclastic units and [intrusive](#)

67 [rocks](#) can be very stiff (high Young's modulus; [from ca. 1.7 to 27 GPa for limestones, Touloukian,](#)  
68 [1981; ca. 5.4 GPa for volcanic rocks, Heap et al., 2020](#)), whereas young and non-welded pyroclastic  
69 units may be very soft (low Young's modulus; [ca. 1.7 – 3.1 GPa, Margottini et al., 2013](#)).  
70 Consequently, the local stress may change abruptly from one layer to another ([e.g., Gudmundsson,](#)  
71 [2006](#)). Irrespective of the scope of the numerical investigation, the importance of applying accurate  
72 rheological constraints to FEM modelling was discussed in many studies ([e.g., Folch et al., 2000;](#)  
73 [Newman et al., 2001; Fernandez et al., 2001; Currenti et al., 2010; Geshi et al., 2012](#)). This implies  
74 that geology of the volcanic area needs to be considered as more accurate as possible. However, few  
75 investigations have been carried out to assess the influence of the amount and quality of geological  
76 data into FEM computations ([Kinvig et al., 2009; Norini et al., 2010, 2019; Cianetti et al., 2012;](#)  
77 [Ronchin et al., 2013; Chaput et al., 2014](#)). To bridge this gap, in this work we use the Linear Static  
78 Analysis (LISA) software (version 8.0; [www.lisafea.com](#)) to study the subsurface stress behaviour in  
79 an elastic domain at Colima Volcanic Complex (CVC, Mexico) when improving the description of  
80 geological constraints.

81 The CVC area is a good candidate for testing the response of FEM software to different geological  
82 conditions, being constituted by a large volcanic complex (significant topographic load; [Lungarini et](#)  
83 [al., 2005](#)), a well-defined feeding system inferred from geophysical and petrological data ([e.g. Spica](#)  
84 [et al., 2017; Massaro et al. 2018, 2019](#)), and growth within a tectonic graben (bordered by normal  
85 faults; [Fig. 1a](#)) infilled by volcanoclastic material (variability of rock mechanical characteristics;  
86 [Norini et al., 2010, 2019](#)).

87 [In this light](#), the present study proposes a contribution to a more proper use of FEM models for  
88 assessing [the stress state](#) pattern in volcanic areas [at different levels of description of the geological](#)  
89 [features](#). [In particular, we focus on the CVC by using the available published data of the inferred](#)  
90 [feeding system structure, in order to assess how the addition of geological and volcanological](#)  
91 [constraints \(i.e. stratigraphy, geometry of the plumbing system, extensional tectonic regime, local](#)  
92 [fault systems\) may, and at what extent, affect the model outputs \(Fig 1b\)](#). Beside and beyond the  
93 evaluation of geological details on FEM outputs, we also obtained a picture of the large-scale stress  
94 distribution in the CVC subsurface.

95

## 96 2 The Colima Volcanic Complex (Mexico)

### 97 2.1 Geological framework

98 The Pleistocene-Holocene CVC is one of the most prominent volcanic edifices within the Trans-  
99 Mexican Volcanic Belt (TMVB) (Macías et al., 2006; Capra et al., 2016; Norini et al., 2019; [Fig. 1a](#)).  
100 In this area, the Rivera microplate and the Cocos plate subduct beneath the North America plate  
101 along the Middle American Trench, producing great deformation and fragmentation of the  
102 continental plate (Stock and Lee, 1994), and forming a triple junction that delimits the tectonic units  
103 known as the Jalisco Block (JB) and the Michoacán Block (MB) (Luhr et al., 1985; Allan, 1986;  
104 Rosas-Elguera et al., 1996; Rosas-Elguera et al., 1997; Ferrari and Rosas- Elguera, 1999; Rosas-  
105 Elguera et al., 2003; Frey et al., 2007). The three rifts of this system are the Tepic-Zacoalco (TZR),  
106 the Chapala-Tula (CTR), and the Colima Rift (CR) where the CVC is emplaced (Allan, 1986;  
107 Escudero and Bandy, 2017). The still active NS trending Colima Rift (CR) was formed during an  
108 extensional phase occurred after the Late Cretaceous–Paleogene compressive and transpressive phase  
109 (Allan, 1986; Serpa et al., 1992; Bandy et al., 1995; Cortés et al., 2010). The rifting phase deformed  
110 Cretaceous marine limestones, Jurassic–Tertiary metamorphosed clastic and volcanoclastic sediments,  
111 Cretaceous–Tertiary intrusive rocks and Tertiary-Quaternary volcanic deposits along sub-vertical  
112 crustal faults. While opening, CR was gradually filled with Pliocene–Quaternary lacustrine sediments,  
113 alluvium and colluvium (e.g. Allan, 1986; Allan et al., 1991; Norini et al., 2010). The geometry,  
114 kinematics and dynamics of the CR have been studied on the basis of field, seismic, and geodetic  
115 data, mainly collected in its northern and central sectors ([see Fig. 1 in Norini et al., 2010](#)).  
116 The amount of vertical displacement of the northern and central sectors is estimated to be at least 2.5  
117 km by adding the topographic relief of the bounding fault scarps (1.5–1.6 km) to the calculated  
118 sediment depth (Allan, 1985; Serpa et al., 1992). Field data and focal mechanism solutions are  
119 consistent with a direction of opening of the northern and central sectors oriented from E-W to NW-  
120 SE, with a mainly normal and minor right-lateral displacements of the bounding faults (Barrier et al.,  
121 1990; Suárez et al., 1994; Rosas-Elguera et al., 1996; Garduño-Monroy et al., 1998; Norini et al.,  
122 2010, 2019). In contrast to field and seismic evidence of long-term slightly dextral oblique extension,  
123 recent GPS geodetic measurements suggest a possible sinistral oblique extension of the CR (Selvans  
124 et al., 2011). In both cases, the stress regime is mainly extensional, with an approximately E-W

125 orientation of the minimum horizontal stress in the basement of the CVC (Barrier et al., 1990; Suárez  
126 et al., 1994; Rosas-Elguera et al., 1996; Selvans et al., 2011; Norini et al., 2010, 2019).

127 The CVC stands within the central sector of the CR, on top of the Cretaceous limestones, Late  
128 Miocene-Pleistocene volcanic rocks, and Pliocene-Holocene lacustrine sediments, alluvium, and  
129 colluvium (Allan, 1985, 1986, 1991; Cortès, 2005; Norini et al., 2010). The volcanic complex is  
130 affected and displaced by the N-S/NNE-SSW-trending recent-active crustal faults of the CR,  
131 controlling the geometry and location of the volcano feeding system (Fig. 1a). Indeed, the CVC was  
132 formed by three andesitic stratovolcanoes aligned parallel to the CR bounding faults: the northern  
133 inactive Cantaro volcano (2900 m a.s.l.), following by the inactive Nevado de Colima (4255 m a.s.l.)  
134 and, in the southern part, the youngest and active Volcán de Colima (3763 m a.s.l.) (Norini et al.,  
135 2019 and reference therein).

136

## 137 *2.2 Eruptive activity*

138 The eruptive history of the CVC started in the northeast area with the formation of Cantaro volcano  
139 at ca. 1-1.5 Ma. The volcanic activity of the Nevado de Colima started at ca. 0.53 Ma. It is composed  
140 of voluminous andesitic lava domes and flows and pyroclastic deposits associated with caldera  
141 forming eruptions and numerous partial sector collapses (Robin et al., 1987; Roverato et al., 2011;  
142 Roverato and Capra, 2013; Cortès et al., 2019). The youngest Volcán de Colima, now considered one  
143 of the most active volcanoes of the world, consists of the Paleofuego edifice that suffered several  
144 sector collapses, with the formation of a horseshoe-shaped depression where the new active cone  
145 (also known Volcán de Fuego) grew up, through Merapi and Soufrière type dome collapses,  
146 extrusion of lava flows, Vulcanian and occasionally sub-Plinian explosive eruptions (Saucedo et al.,  
147 2010; Massaro et al., 2018, 2019). The activity of both Nevado and Volcán de Colima volcanoes **also**  
148 included several sector collapses, occurred frequently in the Upper Pleistocene and Holocene,  
149 repeatedly devastating the floor of the Colima Rift down to the Pacific Ocean (Robin et al., 1987;  
150 Luhr and Prestegard, 1988; Stoopes and Sheridan, 1992; Capra and Macias, 2002; Cortès, 2005;  
151 Roverato et al., 2011).

152

153 *2.3 The CVC plumbing system*

154 Spica et al. (2017) indicate a 15 km-deep low velocity body (LVB) as the CVC deep magma  
155 reservoir. Its horizontal extension seems to be delimited by the borders of the CR, suggesting a  
156 structural control of the normal fault system on it (Spica et al., 2014). The LVB has an extent of ca.  
157 | 55 km × 30 km in the N-S and E-W directions respectively, showing a mean thickness < 8 km.  
158 Escudero and Bandy (2017) obtained a higher resolution tomographic image of the subsurface in the  
159 CVC area, showing that the most active magma generation zone is presently under the Fuego de  
160 Colima edifice. Here, the ambient seismic noise tomographic study proposed by Spica et al. (2014)  
161 confirmed the presence of a shallow magma chamber above ca. 7 km depth, as also demonstrated by  
162 petrological studies (Medina-Martinez et al., 1996; Luhr, 2002; Zobin et al., 2002; López-Loera et al.,  
163 | 2011; Reubi et al., 2013, 2019; Macías et al., 2017). Cabrera-Gutiérrez and Espíndola (2010)  
164 suggested the shallow active magma storage has a volume of ca. 30 km<sup>3</sup>. The shallow magma  
165 chamber is connected to the surface by a dyke/conduit system, whose path is facilitated by the  
166 presence of the CR fault zone, which provides a natural pathway for fluids (e.g., Allan, 1986; Norini  
167 et al., 2010, 2019). The arrangement of dykes and the alignment of volcanic centres of CVC suggest  
168 that the dykes swarm draining the magma chambers developed along the NNE-SSW-trending, steep,  
169 eastward dipping normal fault exposed on the northern CVC flank (Norini et al., 2010, 2019).

170 Taking into account the previous information, Massaro et al. (2018) provided a first-order  
171 geometrical reconstruction of the Fuego de Colima feeding system during the 1913 sub-Plinian  
172 eruption, by using volcanological data (Saucedo et al., 2010, 2011; Bonasia et al., 2011) as input and  
173 constraints for numerical simulations. Results showed good matches for a hybrid configuration of the  
174 shallow conduit-feeding system (i.e., dyke developing into a shallower cylindrical conduit). The best-  
175 | fit dyke geometry has width in the range from 200 m to 2000 m and thickness of ca. 40 m, with the  
176 cylindrical conduit diameter similar to the dyke thickness. The shallow magma chamber top was set  
177 | at 6 km of depth, and dyke-cylinder transition at 500 m below the summit, as also inferred from  
178 geophysical data (Salzer et al., 2014; Aràmbula et al., 2018).

179

### 180 3 Methods

181 In this study, we used the commercial 8.0 version of LISA software ([www.lisafea.com](http://www.lisafea.com)). LISA is a  
182 general-purpose Finite Element Analysis (FEA) software developed in the '90s based on the  
183 formulations proposed by Rao (1989). Since then, formulations from many other sources **were** also  
184 integrated (Bathe, 1990; Michaeli, 1991; Schwarz, 1991; Babuska et al., 1995). Despite FEA was  
185 originally used for structural analysis (Rao, 1989; 2013), it is also able to successfully predict the  
186 stress-strain behaviour of rock masses accounting for elastic models, in particular the deformation  
187 and failure mechanisms even in layered rock masses (Gabrieli et al., 2015).

188 Simplifying techniques in structural FEA can give valuable insights into local stresses more rapidly  
189 and efficiently than a full 3D model. Here we considered a 2D model throughout a complex structure  
190 (*i.e. dual magma chamber feeding system, rift system, rock layering, and faults*), in order to  
191 investigate the stress behaviour induced in the host rocks in response to the increasing detail of  
192 geological data used to constrain the model.

193

#### 194 *3.1 Modelling approach*

195 Taking into account the works of Norini et al. (2010, 2019), we simulated the **stress field** of the CVC  
196 plumbing system considering an E-W cross-section, which is parallel to the extension associated to  
197 the active Colima Rift (Norini et al., 2010), shown in Figure [1a-b](#) (a-a').

198 Since the **extent** of the CVC magma chambers in the NNE-SSW direction **is** typically much longer  
199 than the dimensions of the E-W cross section (Spica et al., 2017), 2D solutions of either numerical or  
200 analytical models describing E-W elongated magma chambers in the crust can be **reasonably** adopted  
201 (Jaeger et al., 2009; Costa et al., 2011). A topographic profile and 2D plane along the chosen E-W  
202 cross-section of the CVC area was obtained in ESRI ArcGIS from a Digital Elevation Model (DEM;  
203 resolution 50 m; [Instituto Nacional de Estadística y Geografía - INEGI <https://en.www.inegi.org.mx/>](https://en.www.inegi.org.mx/)).

204 This cross section was imported into Autodesk Auto-Cad R13 and approximated to a third-degree  
205 spline. Finally, the IGES file was imported into LISA, where the mesh discretization was performed.

206 The domain was discretized by **three and four-node** finite elements (Table 1; [Fig. 1c](#)). The volcanic

207 area domain extends 60 km horizontally and 30 km below the surface set in an  $x$ - $z$  Cartesian  
208 Coordinate System. Zero normal displacements are assigned at the bottom and the lateral boundaries  
209 of the domain, while the upper boundary representing the ground surface is stress free (Fig. 1c). [The](#)  
210 [analysis is carried out by using a plane strain approximation, implying that the deformation in the](#)  
211 [third direction is assumed to be negligible.](#)

212 FEM of geological structures requires accurate discretization of the computational domain such that  
213 geological units are represented correctly. Zehner et al. (2015) reported that the unstructured  
214 tetrahedral meshes on a complex geological model has to fulfil the following requirements: i)  
215 sufficient mesh quality: the tetrahedrons should not be too acute-angled, since numerical instabilities  
216 can occur, ii) incorporation of geometry for defining boundary conditions and constraints, iii) local  
217 adaption, which is a refinement of the mesh in the vicinity of physical sources in order to avoid  
218 numerical errors during the simulation. Considering these requirements, in this work we adopt as the  
219 best discretization a mesh with 4660 [plane continuum](#) elements for the E-W cross-section. The size of  
220 finite elements was refined in the regions with higher gradients, especially near the contours of the  
221 magmatic feeding systems.

222 In our simulations, the [extent](#) of the [rock layers \(Table 2\)](#) is referred to the model [of](#) Norini et al.  
223 (2010, 2019). Magma chambers and dykes are considered as [pressurized](#) finite-size bodies in an  
224 elastic crustal segment, acting as fluid-filled holes. [The boundary condition \(pressurization\) is](#)  
225 [provided by applying internal forces that act on the walls.](#) This approach has been extensively used in  
226 several analytical and numerical models that treat magma reservoirs as internally pressurized  
227 ellipsoidal cavities within an elastic half space, in order to gain insight into the behaviour of magma  
228 plumbing systems (Pinel and Jaupart, 2004; Gudmundsson, 2006; Grosfils, 2007; Andrew and  
229 Gudmundsson, 2008; Hautmann et al., 2013; Currenti and Williams, 2014; Zhong et al., 2019).

230 The geometrical configuration set for the CVC feeding system (i.e. the shape and dimensions of the  
231 magmatic chambers) derives from [the](#) literature (Spica et al., 2014, 2017; Massaro et al., 2018, 2019)  
232 [and it is simplified in Figure 1d.](#) The overpressure in magma chambers may be produced by a variety  
233 of processes, including fractional crystallization, volatile exsolution and magma recharge, leading to  
234 deviatoric stresses in the country rock that may be tens of MPa in magnitude (Jellinek and DePaolo,  
235 2003; Karlstrom et al., 2010).

236 | Previously published studies indicate that differences between, and problems with, elastic models  
237 | derive principally from the key role played by gravity (e.g. Albino et al., 2018). Gravity plays a first  
238 | order role on bedrock failure conditions (Gerbault, 2012), on the geometry of magma propagation  
239 | with respect to an edifice load and on buoyancy contrasts driving magma upward (Lister and Kerr,  
240 | 1991; Watanabe et al., 2002). However, in a wide variety of simulations of natural phenomena the  
241 | gravitational effects are often incorporated either incorrectly or incompletely (e.g. Grosfils, 2007).  
242 | Some authors argued on whether it is appropriate or not to account for the gravity body force in  
243 | numerical models of volcanic inflation (e.g. Currenti and Williams, 2014; Grosfils et al., 2015).  
244 | When the gravitational loading is not included in the model, the volcanic deformation results from a  
245 | change with respect to a stage previously at equilibrium (e.g. Gerbault et al. 2018). In this work, we  
246 | carried out simulations considering the effect of the gravitational loading. Gravity in the host rock is  
247 | implemented via body forces. The model initial condition has a pre-assigned lithostatic stress, whose  
248 | computation, in presence of topography and material heterogeneities, is not trivial because it requires  
249 | applying the gravity load preserving the original not deformed geometry of the mesh (Cianetti et al.,  
250 | 2012). Since the presence of a lithostatic stress field, the load applied at the reservoir boundaries  
251 | represents a superposition of the magmatic overpressure and lithostatic component.  
252 | We also took into account the effect of the existing faults of the Colima Graben (CG) system even if  
253 | LISA cannot include a frictional law to represent the fault movement (i.e. Chaput et al., 2014). As  
254 | reported in Jeanne et al. (2017 and reference therein) the damage induced by faults increases from the  
255 | host rocks to the fault core implying the reduction in the effective elastic moduli represented by a  
256 | progressive decrease in Young's Modulus. Considering the evaluation of fault zone elastic properties  
257 | provided by Jeanne et al. (2017), we represented the faults bordering the CG as two damage zones  
258 | inclined of ca. 70° and with a thickness of ca. 1 km, showing reduced elastic properties with respect  
259 | to the surrounding host rocks down to 10 km in depth.  
260 | It is important to note that we chose to represent the different simulations using different colour  
261 | scales. Although such a choice makes more difficult a visual comparison of the simulation outputs  
262 | and it needs to be kept in mind looking at the different figures, it preserves the necessary details of



263 [stress distribution, which would have been lost using a common colour scale for all the figures in](#)  
264 [LISA.](#)

265

## 266 **4 Geological data**

267 In this work, we used geological information available in literature as input data, in order to estimate  
268 the stress variations around the CVC magmatic plumbing system. Here we briefly describe the main  
269 geological features taken into account in LISA simulations.

### 270 *4.1 Stratigraphy*

271 [Four](#) units forming the CVC system were defined from the available geological data (Table 2): i)  
272 Basement (Unit B): cretaceous limestones and intrusive rocks forming the bed-rock underlying the  
273 CVC; ii) Graben fill deposits (Unit GF): Quaternary alluvial, colluvial, and lacustrine deposits filling  
274 the graben; iii) Fuego de Colima deposits (Unit FC): andesitic lavas and pyroclastic deposits forming  
275 the Paleofuego-Fuego de Colima edifices; [and](#) iv) Volcaniclastic deposits (Unit VD): volcaniclastic  
276 deposits covering the southern flank of the CVC (e.g. Cortés et al. 2010; Norini et al., 2010, 2019).  
277 Being the area interested by FEM extended down to 30 km, it is evident how Unit B is dominant with  
278 respect to the others, which occupy only few km in the upper part of the simulated domain. We  
279 assumed constant mechanical characteristics within each Unit (Table 2). In particular, Unit B was  
280 considered mechanically homogeneous with elastic properties of a carbonate, due to the lack more  
281 detailed information of deeper lithologies (Norini et al., 2019).

282 Deformation within the brittle upper crust is described by elastic material behaviour. For each Unit  
283 we fixed typical rock mass properties, density ( $\rho$ ), Young's Modulus (E) and Poisson's Ratio ( $\nu$ )  
284 (Table 2). The rock masses are considered dry, in order (eventual) pore pressure to be neglected.  
285 Only for Unit GF a higher value for the Poisson's Ratio was used close to the surface in order to  
286 mimic high water content in the graben sediments. The maximum thickness of the graben fill (about  
287 1 km) was assumed from the literature (Allan, 1985; Serpa et al., 1992; Norini et al., 2010, 2019). For  
288 Units B and GF rock mass proprieties were derived from Hoek and Brown (1997) and Marinos and  
289 Hoek (2000), while for volcanic materials (units FC and VD; Table 2) were estimated according to

290 the approach proposed by Del Potro and Hürlimann (2008). This information allowed Norini et al.  
291 (2019) to derive the equivalent Mohr-Coulomb properties for the stress ranges expected in the  
292 different sectors of the CVC. In addition, in order to describe the effects of the CG faults on stress  
293 field distribution, the mechanical properties were locally degraded in proximity of the faults  
294 themselves.

#### 295 *4.2 The geometry of the plumbing system*

296 The geometry of the E-W cross-section of the CVC plumbing system was modelled taking into  
297 account the previous subsurface information described in Section 4.1. In our 2D model, we assumed  
298 the CVC composed of a two magma chambers connected by dykes and to the surface by a conduit  
299 (Fig. 1d). The shape of the magma chambers and dykes are represented by elliptical cross-sections  
300 with the major (*2a*) and minor (*2b*) axes.

301 Generally, the magma chambers have a sill-like shape that is often imaged in seismic studies of  
302 volcanoes and rift zones (Macdonald, 1982; Sinton and Detrick, 1992; Mutter et al., 1995; MacLeod  
303 and Yaouancq, 2000; Singh et al., 2006; Canales et al., 2009). Most of them are not totally molten but  
304 rather a mixture of melt and crystal mush (i.e. Parfitt and Wilson, 2008). Various estimates have been  
305 made to infer the actual amount of melt in a magmatic body, showing that it is only ca. 10% of the  
306 total chamber volume (Gudmundsson et al., 2012 and reference therein).

307 Spica et al. (2017) described a 15 km-deep low velocity body (LVB) with its top at ca. 15 km of  
308 depth and with an estimated volume of ca. 7000 km<sup>3</sup>, representing the deep magmatic reservoir of  
309 CVC. Assuming the melt as 10%, the deep magma chamber volume would be ca. 700 km<sup>3</sup>.  
310 Simplifying this volume in an elliptical sill-like geometry, the dimensions (i.e. *2a*, *2b*, *2c* axes) have  
311 to be scaled according to those of LVB (55 × 30 × 8 km; Spica et al., 2017). We therefore fixed *2a* =  
312 14 km, *2b* = 3.6 km, *2c* = 26 km as the dimensions of the deep magma chamber, being *2c* elongated  
313 in NW-SE direction.

314 For the shallow part of the feeding system, we have no detailed geophysical constraints. However,  
315 Massaro et al. (2019) reproduced through numerical modelling the nonlinear cyclic eruptive activity  
316 at Fuego de Colima in the last 20 years, using a shallow magma chamber volume in the range of 20-  
317 50 km<sup>3</sup>, also according to the estimation of Cabrera-Gutiérrez and Espindola (2010). Assuming a

318 volume of  $30 \text{ km}^3$ , we fixed  $2a = 3.5 \text{ km}$ ,  $2b = 2 \text{ km}$ ,  $2c = 8 \text{ km}$  as dimensions of the shallow magma  
319 chamber.

320 Numerous theoretical and field studies have established that host rock stresses dictate the magma  
321 pathways (e.g. Maccaferri et al., 2011; Gudmundsson, 2011). During ascent to the surface, the dykes  
322 align themselves with the most energy-efficient orientation, which is roughly perpendicular to the  
323 least compressive principal stress axis  $\sigma_3$  (e.g. Gonnermann and Taisne, 2015; Rivalta et al., 2019),  
324 [providing the magma driving pressure remains small compared to the deviatoric stress \(Pinel et al.,](#)  
325 [2017; Maccaferri et al., 2019\)](#). This behaviour, however, can be modulated in the presence of  
326 significant variations in fracture toughness of the surrounding rock due to stratification (Maccaferri et  
327 al., 2010) or to old and inactive fracture systems (Norini et al., 2019). Although for oblate magma  
328 chambers the propagation of dykes is most probable from the tip areas, in our simulations the  
329 orientation of dykes is assumed vertical, because of the preferential pathways represented by the CR  
330 fault planes (Spica et al., 2017).

331 Although, for decades, magma conduits were modelled as cylinders, because of easiness of their  
332 mathematical treatment, geophysical data and field observations highlight the importance [and](#)  
333 [peculiarities](#) of dykes in magma transport and hence the need to adopt more realistic geometries  
334 (Costa et al., 2009; Hautmann et al., 2013; Tibaldi, 2015). It is important to stress that although all  
335 cavities/inclusions in a medium modify the local stress field and concentrate stresses, the induced  
336 perturbation depends mainly on the geometry of the cavity/inclusion (Savin, 1961; Boresi [et al.](#),  
337 1985; Tan, 1994; Saada, 2009). We set the dimensions of feeder dykes in agreement with Massaro et  
338 al. (2018): deep dyke  $2ad = 2 \text{ km}$ ; shallow dyke  $2a$  varies from 1 km at bottom to 500 m in the upper  
339 part of the volcano; width of both deep and shallow dyke  $2bd = 2b = 100 \text{ m}$  [\(Fig. 1d\)](#), [although the](#)  
340 [exact value of the latter is not crucial for the purposes of this study](#). [Moreover,](#) it is worth noting that  
341 it is not the aim of this [work](#) to provide the conditions for the magma chamber rupture, being LISA  
342 accounting only for the elastic regime. For these reasons, the selected magma overpressures ( $\Delta P$ )  
343 [acting on the magma reservoirs and dykes](#) have to be less than the tensile strength of the rocks. We  
344 therefore fixed  $\Delta P$  at 10 MPa and 20 MPa for the 15 km-deep chamber, and 5 MPa for the 6 km-deep  
345 one. For the dykes and conduit, the magmatic overpressure is fixed at 10 MPa in the deeper dyke and  
346 5 MPa in the shallower dyke, except for the upper 500 m of the shallower [conduit](#) where overpressure

347 is set at 0.4 MPa.

348 To take into account the effect of both far field extensive regime and CG around the magma feeding  
349 system, we applied a uniform extension at the lateral boundaries of the domain (as reported in Martì  
350 and Geyer, 2009) of 5 MPa and included two damage zones with reduced rock elastic moduli and  
351 density (i.e.  $E = 1$  GPa,  $\nu = 0.20$ ; Jeanne et al., 2017;  $\rho = 1850$  kg/m<sup>3</sup>).

352

353

## 354 **5 Results**

355 The first part of this section is focused on a sensitivity analysis of Young modulus variation, aimed to  
356 quantify the numerical effects of approximation of this important rock property on FEM outputs. The  
357 second part of this section describes the model outputs when adding complexity to the input  
358 geological/geophysical data.

359 Considering the E-W cross-section (a-a'; Fig. 1a), we provided six domain configurations with  
360 increasing geological complexity: i) "*homogeneous lithology model*" in which the volcanic domain is  
361 only composed of andesite rocks; ii) "*not homogeneous lithology model*" where different geological  
362 units are considered; iii) "*single magma chamber model*" composed of a not homogeneous lithology  
363 and a 15 km-deep magma chamber; iv) "*dual magma chamber model*" composed of a not  
364 homogeneous and 6 km- and 15 km-deep magma chambers; v) "*conduit feeding system model*"  
365 composed of not homogeneous lithology, 6 km- and 15 km-deep magma chambers connected  
366 through a deep-dyke, and a shallow conduit connecting to the surface; vi) "*extensional model*", in  
367 which we added a 5 MPa horizontal extensional stress (far field) and, vii) "*faulted model*", in which  
368 two damaged zones mimicking the CG faults were added to the "*extensional model*" (local stress)  
369 (Fig. 1b).

370 The number of nodes in the *only substratum* and *single magma chamber* models is set at 4426, for the  
371 dual magma chamber model is set at 4161, and at 3737 for the *conduit feeding system* and *faulted*  
372 models.

373 *5.1 Sensitivity analysis on selected input parameters*

374 In order to quantify the influence of Young Modulus selection on the model outputs, we performed a  
375 sensitivity test using the single magma chamber model as reference case. We evaluated the influence  
376 of varying the Young Modulus in each geological Units on the principal stresses  $\sigma_1$  and  $\sigma_3$ . Taking  
377 into account the material properties used in the simulations (Norini et al., 2010, 2019; Table 2) as  
378 reference values, we compared the stress state of the computational domain at changing ( $\pm$ ) Young  
379 Modulus by an order of magnitude. This variation has been separately applied to each Unit, in order  
380 to assess what is the effect of changing material properties on model outputs. This sensitivity analysis,  
381 although incomplete, may lead to raise awareness on the selection of input data when running a FEM.

382 The sensitivity analysis was carried out on a reduced simulation domain ([the x-axis was set to 35 km](#))  
383 in order to diminish the influence of binding effects that are present along domain borders.

384 We used the Euclidean norm (L2) method for illustrating the results of the sensitivity analysis. The  
385 L2 norm applied on a vector space  $x$  (having components  $i = 1, \dots, n$ ) is strongly related with the  
386 Euclidean distance from its origin, and is equal to:

387

$$388 \quad ||x||_2 = \sqrt{\sum_i^n xi^2} \quad (1)$$

389

390 In our case, the vector space  $x$  is composed of all nodes of the computational domain (Table 1). We  
391 defined  $x_{ref}$  the vector containing the results for the maximum and minimum principal stress when  
392 using the selected values of material properties (Table 1) and  $x(-)$ ,  $x(+)$  the vectors at varying the  
393 Young Modulus of one order of magnitude in each Unit.

394 We evaluated the global variation of stress in the proposed geometrical configurations of the domain  
395 (i.e. not homogeneous lithology, single magma chamber, dual magma chamber, and dual magma  
396 chamber with conduits models) calculating the global relative variation in L2 as follow:

397

$$398 \quad L2(-) = \frac{||x_{ref} - x(-)||_2}{||x_{ref}||_2} \quad (2)$$

$$399 \quad L2(+) = \frac{||x_{ref} - x(+)||_2}{||x_{ref}||_2} \quad (3)$$

400 In Figure 2 are reported the global relative variations in L2 of the principal maximum stress  $\sigma_1$  and  
401 principal minimum stress  $\sigma_3$  caused by the variation of Young's Modulus in each Unit. All the  
402 geometric configurations show variability less than 15%, with few exceptions within Unit B that have  
403 variability over 30% (Fig. 2). It is worth noting that the spatial distribution of the major variations  
404 seems to not significantly affect the final stress distributions, because: i) they are located near the  
405 mesh borders (Fig. 3a, b); and, ii) when not at the mesh borders, the variations are limited to few %  
406 (Fig. 3c, d). It means that changing the Young's Modulus of one order of magnitude produces  
407 variation in FEM outputs distributed over a large domain and the change affecting the single nodes is  
408 limited to few %.

409

### 410 *5.2 Homogeneous and not homogeneous lithology*

411 We carried out LISA simulations considering the effect of the gravitational loading on the  
412 homogeneous and not homogeneous lithology on FEM outputs. In Figure 4 we reported a gravity  
413 loading model for E-W cross-section of the CVC system. We first considered the homogeneous rock  
414 composition composed by only andesitic lavas (Fig. 4a) and then by carbonates (Unit B), alluvial,  
415 volcanoclastic and pyroclastic deposits (Units GF and VD; Fig. 4b). We analysed the principal  
416 stresses  $\sigma_1$  and  $\sigma_3$  acting on the system, which correspond to the maximum and minimum stress at  
417 a point, respectively.

418 Figure 4 shows the patterns of the minimum principal stress  $\sigma_3$  (panels i-ii) and of the maximum  
419 principal stress  $\sigma_1$  (panels iii-vi), highlighting very slight differences between the homogeneous and  
420 not homogeneous lithology cases. It is very important to stress that the  $x$ - $z$  zero displacement  
421 assigned at the bottom and the lateral boundaries of the domain created substantial artefacts in the  
422 results (i.e. curved patterns of stress). The artefacts are also evident when considering  $\sigma_3$  (panels i-ii)  
423 where the boundary effect on  $x$ -axis is amplified by the presence of the upper free surface. For this  
424 reason, the only area to be considered as unperturbed is the central part of the entire domain, and it  
425 extends ca. 30 km horizontally and ca. 15 km vertically (within the blue contour in Fig. 4).

426

### 427 *5.3 Gravitational modelling using the inferred feeding system geometry*

428 We progressively add the elements of the conduit/feeding system of the CVC to FEM under the  
429 effect of the gravitational loading. Three cross-section profiles (Figs. 5, 6) show increasing  
430 complexity of the feeding system starting from a single magma chamber, passing to two magma  
431 chambers, then adding the conduits, and, finally, considering the effects of faults.

432 Figure 5a describes the distribution of the minimum principal stress  $\sigma_3$  (panel i) and the maximum  
433 principal stress  $\sigma_1$  (panel ii) at magma chamber overpressure of 10 MPa, showing how the insertion  
434 of the pressurized magma chamber modifies the lithostatic stress. No significant differences in  
435 magnitude and pattern of stresses are visible when having a magma chamber overpressure of 20 MPa  
436 (Appendix 1a).

437 The addition of the shallow magma chamber significantly changes the values and pattern of both  $\sigma_3$   
438 and  $\sigma_1$  (Fig. 5b). In particular,  $\sigma_3$  and  $\sigma_1$  stresses describe a typical inflation pattern produced by  
439 overpressurised magma chamber(s) (Anderson, 1936; Gudmundsson, 2006), producing well-defined  
440 stress arches of  $\sigma_3$  (red dotted lines in Figs. 5bi) and divergent strong gradients of  $\sigma_1$ , well developed  
441 around the larger magma chamber (Fig. 5bii). Stress arch is a common phenomenon occurring in  
442 continuous materials as response to applied pressure. It has been proved to have great influences on  
443 the self-stabilization of soils or rock masses (Huang and Zhang, 2012), and may influence  
444 mechanisms of caldera collapse (Holohan et al., 2015). Very slight differences in magnitude and  
445 pattern of stresses appear when using 10 MPa (Fig. 5b) or 20 MPa of deep magma chamber  
446 overpressure (Appendix 1b).

447 Figure 6 shows the effect of adding two conduits connecting the deep and shallow magma chambers.  
448 It is evident how the insertion of the conduits in the feeding system of CVC dramatically changes the  
449 stress distribution, with disappearance of the stress arch and an almost constant stress in the  
450 computational domain except than on the tips of the deep magma chamber.

451

#### 452 *5.4 Extensional field stress*

453 In order to explore the influence of the extensional far field stress on stress patterns (Fig. 1a), we run  
454 simulations applying 5 MPa of extensional stress to the FEM domain, which is a typical low value for

455 rift zones (Turcotte and Schubert, 2002; Moeck et al., 2009; Maccaferri et al., 2014; Sulpizio and  
456 Massaro, 2017; Fig. 7).

457 In the case of a single magma chamber (with 10 MPa overpressure; Fig. 7, panels i-ii), the addition of  
458 extensional far field stress reduces the confinement effect due to the no displacement condition  
459 imposed along the  $x$ - $z$  directions (plane strain approximation). The effect of the extensional field  
460 stress on double magma chamber configuration (with 10 MPa overpressure in the deep chamber and  
461 5 MPa in the shallower one) produces slight changes in stress magnitude and pattern for both  $\sigma_3$  and  
462  $\sigma_1$  (Fig. 7, panels iii-iv) with respect to Figure 5b. The same applies also for the complete feeding  
463 system configuration, in which the attrition of the far field stress slightly changes the intensity of the  
464 stresses and patterns (Fig. 7, panels v-vi). Using 20 MPa overpressure in the deep magma chamber  
465 does not significantly affect the model outputs (Appendix 2).

466

#### 467 *5.5 Faults bordering the Colima Rift*

468 In order to reproduce the effect of faults bordering the Colima Rift on the final feeding system  
469 configuration, we added two damage zones by degrading the elastic properties of a volume of rock  
470 mass.-The insertion of the two zones of weakness does not alter significantly the stress distribution  
471 observed in Figures 7v and 7vi, with only reduction of both  $\sigma_1$  and  $\sigma_3$  values in the surroundings of  
472 the damage zones (Figs. 7vii and 7viii). The different distance of the two damage zones to the  
473 feeding system (especially the deep magma chamber) produces a small asymmetry in both  $\sigma_1$  and  $\sigma_3$   
474 patterns with respect to simulations without damage zones (Figs. 7v-viii).

475

476

## 477 **6 Discussions**

478

### 479 *6.1 FEM analysis at increasing geological details*

480 The presented FEM model of the CVC highlighted some important characteristics of crustal stress  
481 distribution at changing geological constraints used as input conditions (Spica et al., 2014, 2017;  
482 Massaro et al., 2018). Although the results have to be considered as a first order approximation, the



483 changes in stress distribution are evident and useful for the understanding of limitations and  
484 advantages of [FEM](#).

485 Under the assumptions [of plane strain, gravitational loading, and overpressured magma chambers and](#)  
486 [dykes](#), the use of homogeneous or not homogeneous lithology for FEM provides negligible effects in  
487 stress intensity and pattern (Fig. 4). This is because the upper Units (Units FC, VD, GF; Table 2)  
488 represent only a limited part of the simulated domain, which in the remaining part results entirely  
489 composed of the assumed homogeneous basement (Unit B; Table 2). This does not mean that the  
490 influence of the upper Units may be still negligible using smaller scales of the simulated domain.

491 Analysing the FEM outputs with the single magma chamber, it emerges how [the overpressures,  \$\Delta P\$](#) ,  
492 only limited the effects of gravitational loading. The use of a dual magma chamber geometry better  
493 describes the inflation induced by overpressure within magma chambers, with the formation of the  
494 stress arch in the minimum compressive stress  $\sigma_3$  plot. It is important to highlight that for both single  
495 and dual magma chamber models, the change of internal overpressure from 10 to 20 MPa slightly  
496 changes the magnitude of the stress but not their general patterns (Appendix 1-2).

497 The presence of [dykes](#) in the magma feeding system dramatically change the  $\sigma_3$  and  $\sigma_1$  patterns (Fig.  
498 6). Indeed, they become quite homogeneous throughout the computational domain, with the only  
499 exception of sidewall effects induced by the zero displacement conditions, already discussed in  
500 Figure 4.

501 The addition of extensional field stress of 5 MPa reduces the sidewall effects and produces an almost  
502 homogeneous stress distribution in the upper part of the [computational](#) domain, above the top of the  
503 deep magma chamber. [This, along with the additional inclusion of the damage zones introduced to](#)  
504 [mimic the effects of CG faults](#), describes a close to equilibrium volcanic system, in which volcanic  
505 overpressure and lithostatic stress almost equilibrate each other (Sulpizio et al., 2016).

## 506

### 507 *6.2 Some implication of the stress state of the CVC inferred from FEM*

508 The results obtained with the insertion of the full feeding system and far field stress on the FEM  
509 highlight an almost homogeneous stress distribution in the CVC area. This means that the shape of  
510 the dual magma chamber [feeding system](#) model and far field stress provide a stable geometry, which  
511 limits the stress changes to few MPa. All the large stress variations are located at the tips of the

512 magma chambers, as expected for pressurized or under-pressurized cavities in the lithosphere (Martì  
513 and Geyer, 2009). This means that the whole feeding system is in a quasi-equilibrium state, and, as  
514 an example, any overpressure created by input of new magma is adjusted by increasing the magma  
515 chamber volume or erupting at the surface. Even if we consider the scenario of complete emptying  
516 the upper conduit and part of the shallow magma chamber, as occasionally occurred during the past  
517 sub-Plinian and Plinian eruptions (Luhr et al., 2002; Saucedo et al., 2010; Massaro et al., 2018), this  
518 would result in the restoration of the stress arch, which is still a stable stress configuration. Even the  
519 complete emptying of the shallow magma chamber probably would be ineffective for triggering a  
520 large collapse (caldera forming) of the feeding system. This latter event would be possible only if a  
521 large depressurization of the deeper magma chamber would occur, but it implies the eruption of tens  
522 to hundreds of km<sup>3</sup> of magma, which seems not very likely provided the current stress distribution in  
523 CVC.

524 Beside and beyond the limitations due to the first order approximation of the FEM analysis, other  
525 sources of uncertainties in the discussion about present and future stress state of the CVC come from  
526 not considering gravity-driven processes, such as volcano spreading due to plastic deformation of the  
527 GF Unit (Norini et al., 2010, 2019) or pressurization of the shallower conduit (Massaro et al., 2018),  
528 and detailed regional tectonics (Norini et al., 2010, 2019). The effect of the two fault systems  
529 bordering the Colima Rift were simulated by degrading the mechanic properties of rocks in an area of  
530 about 1 km width up to a depth of 10 km. Although the effects are negligible at the scale of the  
531 computational domain, it cannot be excluded some local significant effects that cannot be resolved  
532 using the described approach.

533

## 534 **7 Conclusions**

535 The increasing details of geological and geophysical data to FEM simulation at Colima Volcanic  
536 Complex (Mexico) showed the importance of using the most accurate input data in order to have  
537 reliable outputs. In particular, the data here presented highlighted how the use of simplified models  
538 produces unreliable outputs of the stress state of the volcano subsurface.

539 Beside and beyond the results obtained by analysing the influence of detailing geological and  
540 geophysical data, the FEM of CVC confirms the close to equilibrium state of the volcano, which is  
541 the expected stress distribution induced by a feeding system directly connected to the surface.  
542 This means that any overpressure created by input of new magma is adjusted within the feeding  
543 system, sometimes triggering eruptions. The complete emptying the upper conduit and part of the  
544 shallow magma chamber, as occasionally occurred in the past, originating sub-Plinian and Plinian  
545 eruptions, would result in the restoration of the stress arch, which is still a stable stress configuration.  
546 Descends that large magnitude, caldera forming eruptions are possible only if the **bigger** deep magma  
547 chamber is **also** involved and significantly emptied during an eruption.

548

## 549 **Appendices**

550

### 551 **Appendix 1**

552 E-W gravitational modelling of the CVC domain (stratified lithology) for all configurations  
553 investigated. The magnitude and pattern of the principal stress account for a) single magma chamber  
554 model ([number of nodes: 4426](#)); b) dual magma chamber model ([number of nodes: 4161](#)); c) dual  
555 magma chamber with conduits model ([number of nodes: 3737](#)). [The dimension of the deep magma](#)  
556 [chamber:  \$2a = 14\$  km and  \$2b = 3.6\$  km at 15 km of depth; shallow magma chamber:  \$2a = 3.5\$  km and](#)  
557  [\$2b = 2\$  km at 6 km. The magmatic overpressure is 20 MPa for the deep chamber, and 5 MPa for the](#)  
558 [shallower. Black dotted lines highlight the passage from different stress values. Note that the scale of](#)  
559 [stress values are different for each panel in order to maximise the simulation details.](#)

560

### 561 **Appendix 2**

562 E-W gravitational modelling of the CVC domain (stratified lithology) considering a far extensional  
563 stress field of 5 MPa for all configurations investigated. The magnitude and pattern of the principal  
564 stress account for a) single magma chamber model ([number of nodes: 4426](#)); b) dual magma  
565 chamber model ([number of nodes: 4161](#)); c) dual magma chamber with conduits model ([number of](#)  
566 [elements: 3737](#)). [The dimension of the deep magma chamber:  \$2a = 14\$  km and  \$2b = 3.6\$  km at 15 km](#)  
567 [of depth; shallow magma chamber:  \$2a = 3.5\$  km and  \$2b = 2\$  km at 6 km. The magmatic overpressure](#)  
568 [is 20 MPa for the deep chamber, and 5 MPa for the shallower. Black dotted lines highlight the](#)  
569 [passage from different stress values. The red arrows indicate the direction of the applied far field](#)

570 [stress. Note that the scale of stress values are different for each panel in order to maximise the](#)  
571 [simulation details.](#)

572

### 573 **Code/Data Availability**

574 The LISA code is available at <https://lisafea.com/>.

575

### 576 **Author's contribution**

577 [SM, RS, AC, GN and GG conceived the study.](#) SM and RS wrote the [bulk of the](#) manuscript with the  
578 input of all the co-authors. SM and GL compiled the numerical simulations and formulated the  
579 adopted methodology. MP and SM carried out the sensitivity analysis. RS, AC, SM, GN, GG, LC,  
580 GL, MP and AG worked on the interpretation of the results.

581

582 **Competing interests:** The authors declare that they have no conflict of interest.

583 **Acknowledgements:** SM thanks the LISA customer service for the support received.

### 584 **References**

585 Albino, F., Pinel, V., and Sigmundsson, F., 2010. Influence of surface load variations on eruption  
586 likelihood: application to two Icelandic subglacial volcanoes, Grímsvötn and Katla. *Geophysical*  
587 *journal international*, 181(3), 1510-1524.

588

589 Albino, F., Amelung, F., and Gregg, P., 2018. The role of pore fluid pressure on the failure of magma  
590 reservoirs: insights from Indonesian and Aleutian arc volcanoes. *Journal of Geophysical Research:*  
591 *Solid Earth*, 123(2), 1328-1349.

592

593 Anderson E.M., 1936. The dynamics of formation of cone sheets, ring dykes and cauldron  
594 subsidence. *Proc R Soc Edinburgh* 56:128–163.

595

596 Allan, J.F., 1985. Sediment depth in the NCG from 3-D interpretation of gravity. *Geofis. Int.* 24, 21–  
597 30 (1985).

598 Allan, J.F. 1986. Geology of the Northern Colima and Zacoalco grabens, Southwest Mexico: Late  
599 Cenozoic rifting in the Mexican Volcanic Belt. *Geol. Soc. Am. Bull.* 97, 473–485

600 Allan, J.F., Nelson, S.A., Luhr, J.F., Charmichael, I.S.E., Wopat, M., Wallace, P.J., 1991: Pliocene-  
601 Holocene rifting and associated volcanism in Southwest Mexico: an exotic terrane in the making. In:  
602 Dauphin, J.P., Simoneit, R.R.T. (eds.) *The Gulf and Peninsular Provinces of the Californias*, AAPG  
603 *Mem.*, vol. 47, pp. 425–445.

- 604 Andrew, R.E., and Gudmundsson, A., 2008. Volcanoes as elastic inclusions: Their effects on the  
605 propagation of dykes, volcanic fissures, and volcanic zones in Iceland. *Journal of Volcanology and*  
606 *Geothermal Research*, 177(4), 1045-1054.
- 607
- 608 Arámbula-Mendoza, R., Reyes-Dávila, G., Dulce, M.V.B., González-Amezcuca, M., Navarro- Ochoa,  
609 C., Martínez-Fierros, A., and Ramírez-Vázquez, A., 2018. Seismic monitoring of effusive-explosive  
610 activity and large lava dome collapses during 2013–2015 at Volcán de Colima, Mexico. *J. Volcanol.*  
611 *Geotherm. Res.*, 351, 75-88.
- 612 Babuška, I., Ihlenburg, F., Paik, E. T., and Sauter, S.A., 1995. A generalized finite element method  
613 for solving the Helmholtz equation in two dimensions with minimal pollution. *Computer methods in*  
614 *applied mechanics and engineering*, 128(3-4), 325-359.
- 615
- 616 Bandy, W.L., Mortera-Gutiérrez, C.A., Urrutia- Fucugauchi, J., Hilde, T.W.C, 1995. The subducted  
617 Rivera-Cocos plate boundary: where is it, what is it, and what is its relationship to the Colima Rift?  
618 *Geophys. Res. Lett.* 22, 3075–3078.
- 619 Barrier, B., Bourgois, J., Michaud, F., 1990: The active Jalisco triple junction rift system. *C.R. Acad.*  
620 *Sci. Paris*, 310 (II), 1513–1520.
- 621 Bathe, K. J., Zhang, H., and Ji, S., 1999. Finite element analysis of fluid flows fully coupled with  
622 structural interactions. *Computers and Structures*, 72(1-3), 1-16.
- 623
- 624 Bonafede, M., Parenti, B., Rivalta, E., 2002. On strike-slip faulting in layered media. *Geophysical*  
625 *Journal International*, 149(3), 698-723.
- 626
- 627 Bonasia R, Capra L, Costa A, Macedonio G, Saucedo R., 2011. Tephra fallout hazard assessment for  
628 a Plinian eruption scenario at Volcan de Colima. *J Volcanol Geotherm Res* 203: 12–22.
- 629
- 630 Boresi, A.P., Schmidt, R.J., and Sidebottom, O.M., 1985. *Advanced mechanics of materials* (Vol. 6).  
631 New York et al.: Wiley.
- 632
- 633 Buchmann T. and Conolly P.T., 2007. Contemporary kinematics of the Upper Rhine Graben: A 3D  
634 finite element approach. *Global and Planetary Change* 58, 287–309.
- 635
- 636 Bunney, 2014. *The Effects of Structural Heterogeneities and In-elastic Rheology on Ground*  
*Deformation at Campi Flegrei Caldera, Italy*. PhD Thesis.
- 637
- 638 Cabaniss, H.E., Gregg, P. M., and Grosfils, E.B., 2018. The role of tectonic stress in triggering large  
639 silicic caldera eruptions. *Geophysical Research Letters*, 45, 3889–3895. <https://doi.org/10.1029/2018GL077393> .
- 640
- 641 Cayol, V., and Cornet, F. H., 1998. Effects of topography on the interpretation of the deformation  
642 field of prominent volcanoes: Application to Etna. *Geophysical Research Letters*, 25(11), 1979–1982.  
643 <https://doi.org/10.1029/98GL51512>.
- 644
- 645 Cailleau, B., T.R. Walter, P. Janle, and E. Hauber, 2003. Modeling volcanic deformation in a regional  
646 stress field: Implications for the formation of graben structures on Alba Patera, Mars, *J. Geophys.*  
*Res.*, 108(E12), 5141, doi:10.1029/2003JE002135.
- 647
- 648 Cailleau B., Thomas R. Walter, Peter Janle, Ernst Hauber, 2005. Unveiling the origin of radial  
649 grabens on Alba Patera volcano by finite element modelling *Icarus* 176, 44–56.
- 650
- 651 Cabrera-Gutiérrez, R., and Espíndola, J.M., 2010. The 1998-1999 eruption of Volcán de Colima,  
652 Mexico: an application of Maeda's viscoelastic model. *Geofísica internacional*, 49(2), 83-96.
- 653
- 654 Canales, J.P., Nedimović, M.R., Kent, G.M., Carbotte, S.M., and Detrick, R.S., 2009. Seismic  
655 reflection images of a near-axis melt sill within the lower crust at the Juan de Fuca ridge. *Nature*,  
460(7251), 89.

656  
657 Capra, L., and Macias, J.L., 2002. The cohesive Naranjo debris-flow deposit (10 km<sup>3</sup>): A dam  
658 breakout flow derived from the Pleistocene debris-avalanche deposit of Nevado de Colima Volcano  
659 (México). *Journal of Volcanology and Geothermal Research*, 117(1-2), 213-235.  
660  
661 Capra L, Macías JL, Cortés A, Dávila N, Saucedo R, Osorio-Ocampo S, Arce JL, Galvilanes-Ruiz JC,  
662 Corona-Càvez P, Gàrcia-Sancez L, Sosa-Ceballos G, Vasquez R., 2016. Preliminary report on the  
663 July 10–11, 2015 eruption at Volcán de Colima: Pyroclastic density currents with exceptional runouts  
664 and volume, *J Volcanol Geotherm Res* 310: 39-49.  
665  
666 Cianetti, S., Giunchi, C., and Casarotti, E., 2012. Volcanic deformation and flank instability due to  
667 magmatic sources and frictional rheology: the case of Mount Etna. *Geophysical Journal International*,  
668 191(3), 939-953.  
669  
670 Charco, M., and Galán del Sastre, P., 2014. Efficient inversion of three-dimensional finite element  
671 models of volcano deformation. *Geophysical Journal International*, 196(3), 1441-1454.  
672  
673 Chaput, M., Pinel, V., Famin, V., Michon, L., and Froger, J.L., 2014. Cointrusive shear displacement  
674 by sill intrusion in a detachment: A numerical approach. *Geophysical Research Letters*, 41(6), 1937-  
675 1943.  
676  
677 Cortés, A., 2005. Carta geológica del complejo volcánico de Colima. UNAM, Instituto de Geología.  
678  
679 Cortés, A., Garduño, V.H., Macías, J. L., Navarro-Ochoa, C., Komorowski, J.C., Saucedo, R., and  
680 Gavilanes, J. C. (2010). Geologic mapping of the Colima volcanic complex (Mexico) and  
681 implications for hazard assessment. *Geol Soc Am Spec Pap*, 464, 249-264.  
682  
683 Cortés, A., Komorowski, J. C., Macías, J. L., Capra, L., and Layer, P. W., 2019. Late Pleistocene-  
684 Holocene debris avalanche deposits from Volcán de Colima, Mexico. In *Volcán de Colima* (pp. 55-  
685 79). Springer, Berlin, Heidelberg.  
686  
687 Costa, A., Sparks, R.S.J., Macedonio, G., and Melnik, O., 2009. Effects of wall-rock elasticity on  
688 magma flow in dykes during explosive eruptions. *Earth and Planetary Science Letters*, 288(3-4), 455-  
689 462.  
690  
691 Costa, A., Gottsmann, J., Melnik, O., and Sparks, R. S. J., 2011. A stress-controlled mechanism for  
692 the intensity of very large magnitude explosive eruptions. *Earth and Planetary Science Letters*, 310(1-  
693 2), 161-166.  
694  
695 Currenti, G., Bonaccorso, A., Del Negro, C., Scandura, D., and Boschi, E., 2010. Elasto-plastic  
696 modeling of volcano ground deformation. *Earth and Planetary Science Letters*, 296(3-4), 311-318.  
697  
698 Currenti, G., and Williams, C.A., 2014. Numerical modeling of deformation and stress fields around  
699 a magma chamber: Constraints on failure conditions and rheology. *Physics of the Earth and Planetary*  
700 *Interiors*, 226, 14-27.  
701  
702 Dávila, N., Capra, L., Ferrés, D., Gavilanes-Ruiz, J. C., and Flores, P., 2019. Chronology of the  
703 2014–2016 Eruptive Phase of Volcán de Colima and Volume Estimation of Associated Lava Flows  
704 and Pyroclastic Flows Based on Optical Multi-Sensors. *Remote Sensing*, 11(10), 1167.  
705  
706 Del Potro, R. and Hürlimann, M., 2008. Geotechnical classification and characterization of materials  
707 for stability analyses of large volcanic slopes. *Eng. Geol.* 98(1), 1–17.  
708  
709 Dieterich J.H., and R.W. Decker, 1975. Finite element modeling of surface deformation associated  
with volcanism, *J. Geophys. Res.*, 80, 4094–4102.  
710  
711 Escudero, C.R., and Bandy, W.L., 2017: Ambient seismic noise tomography of the Colima Volcano  
Complex. *Bull. Volcanol.* 79, 13.

- 712 Fernández, J., Tiampo, K. F., Jentzsch, G., Charco, M., and Rundle, J.B., 2001. Inflation or deflation?  
713 New results for Mayon Volcano applying elastic - gravitational modeling. *Geophysical Research*  
714 *Letters*, 28(12), 2349-2352.  
715
- 716 Ferrari, L., Rosas-Elguera, J., Márquez, A., Oyarzun, R., Doblás, M., and Verma, S.P., 1999. Alkalic  
717 (ocean-island basalt type) and calc-alkalic volcanism in the Mexican volcanic belt: A case for plume-  
718 related magmatism and propagating rifting at an active margin?: Comment and Reply. *Geology*,  
719 27(11), 1055-1056.  
720
- 721 Folch, A., Fernández, J., Rundle, J.B., Martí, J., 2000. Ground deformation in a viscoelastic medium  
722 composed of a layer overlying a half-space: a comparison between point and extended sources.  
723 *Geophys. J. Int.* 140 (1), 37–50.
- 724 Frey, H.M., Lange, R.A., Hall, C.M., Delgado-Granados, H., Carmichael, I.S.E., 2007. A Pliocene  
725 ignimbrite flare-up along the Tepic-Zacoalco rift: evidence for the initial stages of rifting between the  
726 Jalisco block (Mexico) and North America. *Geol. Soc. Am. Bull.* 119, 49–64.  
727 <http://dx.doi.org/10.1130/B25950.1>.
- 728 Fujita, E., Kozono, T., Ueda, H., Kohno, Y., Yoshioka, S., Toda, N., and Ida, Y., 2013. Stress field  
729 change around the Mount Fuji volcano magma system caused by the Tohoku megathrust earthquake,  
730 Japan. *Bulletin of volcanology*, 75(1), 679.  
731
- 732 Gabrieli, A., Wilson, L., and Lane, S., 2015. Volcano–tectonic interactions as triggers of volcanic  
733 eruptions. *Proceedings of the Geologists' Association*, 126(6), 675-682.  
734
- 735 Garduño-Monroy, V.H., Saucedo-Girón, R., Jiménez, Z., Gavilanes-Ruiz, J.C., Cortés-Cortés, A.,  
736 Uribe-Cifuentes, R.M. 1998: La Falla Tamazula, límite suroriental del Bloque Jalisco, y sus  
737 relaciones con el Complejo Volcánico de Colima, México. *Revista Mexicana de Ciencias Geológicas*  
738 15(2), 132–144.
- 739 Gelman, S.E., Deering, C.D., Gutierrez, F.J., and Bachmann, O., 2013. Evolution of the Taupo  
740 Volcanic Center, New Zealand: petrological and thermal constraints from the Omega dacite.  
741 *Contributions to Mineralogy and Petrology*, 166(5), 1355-1374.  
742
- 743 Geyer, A., and Martí, J., 2009. Stress fields controlling the formation of nested and overlapping  
744 calderas: implications for the understanding of caldera unrest. *Journal of Volcanology and*  
745 *Geothermal Research*, 181(3-4), 185-195.  
746
- 747 Geyer, A., and Gottsmann, J., 2010. The influence of mechanical stiffness on caldera deformation  
748 and implications for the 1971–1984 Rabaul uplift (Papua New Guinea). *Tectonophysics*, 483(3-4),  
749 399-412.  
750
- 751 Geyer, A., Martí, J., and Villaseñor, A., 2016. First-order estimate of the Canary Islands plate-scale  
752 stress field: Implications for volcanic hazard assessment. *Tectonophysics*, 679, 125-139.  
753
- 754 Gerbault, M., Cappa, F., Hassani, R., 2012. Elasto-plastic and hydromechanical models of failure  
755 around an infinitely long magma chamber. *Geochem. Geophys. Geosyst.* 13, Q03009.  
756 <http://dx.doi.org/10.1029/2011GC003917>.
- 757 Gerbault, M., Hassani, R., Lizama CN, Souche, A., 2018. Three-Dimensional Failure Patterns Around  
758 an Inflating Magmatic Chamber. *Geochemistry, Geophysics, Geosystems*, AGU and the  
759 *Geochemical Society*, In press.
- 760 Geshi, N., Kusumoto, S., and Gudmundsson, A., 2012. Effects of mechanical layering of host rocks  
761 on dike growth and arrest. *Journal of Volcanology and Geothermal Research*, 223, 74-82.  
762
- 763 Grosfils, E.B., 2007. Magma reservoir failure on the terres- trial planets: Assessing the importance of  
764 gravitational loading in simple elastic models, *J. Volcanol. Geotherm. Res.*, 166, 47–75,  
765 doi:10.1016/j.jvolgeores.2007.06.007.

- 766 Grosfils, E.B., McGovern, P. J., Gregg, P.M., Galgana, G.A., Hurwitz, D.M., Long, S.M., Chestler,  
767 S.R., 2015. Elastic models of magma reservoir mechanics: a key tool for investigating planetary  
768 volcanism. *Geol. Soc. London, Spec. Pub.*, 401(1), 239-267.
- 769 Gudmundsson, A., and Brenner, S.L., 2004. How mechanical layering affects local stresses, unrests,  
770 and eruptions of volcanoes. *Geophysical Research Letters*, 31(16).  
771
- 772 Gudmundsson, A., 2006. How local stresses control magma-chamber ruptures, dyke injections, and  
773 eruptions in composite volcanoes, *Earth-Sci.Rev.*, 79(1-2), 1-31.
- 774 Gudmundsson, A., 2011. *Rock fractures in geological processes*. Cambridge University Press.  
775
- 776 Goennermann and Taisne, 2015. *Magma Transport in Dikes*. *The Encyclopedia of Volcanoes*.  
777 <http://dx.doi.org/10.1016/B978-0-12-385938-9.00010-9>.
- 778 Gottsmann, J., Folch, A., and Rymer, H., 2006. Unrest at Campi Flegrei: A contribution to the  
779 magmatic versus hydrothermal debate from inverse and finite element modeling. *Journal of*  
780 *Geophysical Research: Solid Earth*, 111(B7).  
781
- 782 Gutiérrez, F., and Parada, M.A., 2010. Numerical modeling of time-dependent fluid dynamics and  
783 differentiation of a shallow basaltic magma chamber. *Journal of Petrology*, 51(3), 731-762.  
784
- 785 Hautmann, S., Gottsmann, J., Sparks, R.S.J., Costa, A., Melnik, O., and Voight, B., 2009. Modelling  
786 ground deformation caused by oscillating overpressure in a dyke conduit at Soufrière Hills Volcano,  
787 Montserrat. *Tectonophysics*, 471(1-2), 87-95.
- 788 Heap, M. J., Villeneuve, M., Albino, F., Farquharson, J. I., Brothelande, E., Amelung, F., and Baud,  
789 P., 2020. Towards more realistic values of elastic moduli for volcano modelling. *Journal of*  
790 *Volcanology and Geothermal Research*, 390, 106684.  
791
- 792 Hickey, J., Gottsmann, J., and Mothes, P., 2015. Estimating volcanic deformation source  
793 parameters with a finite element inversion: The 2001-2002 unrest at Cotopaxi volcano, Ecuador, J.  
794 *Geophys.Res. Solid Earth*, 120, 1473-1486, doi:10.1002/2014JB011731.
- 795 Hoek, E. and Brown, E.T, 1997. Practical estimates of rock mass strength. *Int. J. Rock Mech. Min.*  
796 *Sci.* 34, 1165-1186.
- 797 Holohan, E.P., Schöpfer, M. P. J., and Walsh, J.J., 2015. Stress evolution during caldera collapse.  
798 *Earth and Planetary Science Letters*, 421, 139-151.
- 799 Huang, X., and Zhang, Z., 2012. Stress arch bunch and its formation mechanism in blocky stratified  
800 rock masses. *Journal of Rock Mechanics and Geotechnical Engineering*, 4(1), 19-27.  
801
- 802 Karlstrom, L., Dufek, J., Manga, M., 2010. Magma chamber stability in arc and continental crust. J.  
803 *Volcanol. Geotherm. Res.* 190, 249-270.  
804
- 805 Kinvig, H. S., Geyer, A., and Gottsmann, J., 2009. On the effect of crustal layering on ring-fault  
806 initiation and the formation of collapse calderas. *Journal of Volcanology and Geothermal Research*,  
807 186(3-4), 293-304.  
808
- 809 Jaeger, J.C., Cook, N.G., and Zimmerman, R., 2009. *Fundamentals of rock mechanics*. John Wiley  
810 and Sons.  
811
- 812 Jeanne, P., Guglielmi, Y., Rutqvist, J., Nussbaum, C., and Birkholzer, J., 2017. Field characterization  
813 of elastic properties across a fault zone reactivated by fluid injection. *Journal of Geophysical*  
814 *Research: Solid Earth*, 122(8), 6583-6598.  
815
- 816 Jellinek, A.M. and DePaolo, D.J., 2003. A model for the origin of large silicic magma chambers:  
817 precursors of caldera-forming eruptions. *Bull. Volcanol.* 65, 363-381.



- 818  
819 Lister, J.R. and Kerr, R.C., 1991. Fluid-mechanical models of crack propagation and their application  
820 to magma transport in dykes. *Journal of Geophysical Research* 96,10,049–10,077.
- 821 Long, S.M., and Grosfils, E.B., 2009. Modeling the effect of layered volcanic material on magma  
822 reservoir failure and associated deformation, with application to Long Valley caldera, California.  
823 *Journal of Volcanology and Geothermal Research*, 186(3-4), 349-360.  
824
- 825 López-Loera, H., Urrutia-Fucugauchi, J., Alva-Valdivia, L., 2011. Estudio aeromagnético del  
826 complejo volcánico de Colima, occidente de México – implicaciones tectónicas y estructurales.  
827 *Revista Mexicana de Ciencias Geológicas* 28, 349–370.
- 828 Lungarini, L., Troise, C., Meo, M., and De Natale, G., 2005. Finite element modelling of topographic  
829 effects on elastic ground deformation at Mt. Etna. *Journal of volcanology and geothermal research*,  
830 144(1-4), 257-271.
- 831 Luhr, J.F., and Carmichael, I.S., 1985. Contemporaneous eruptions of calc-alkaline and alkaline  
832 magmas along the volcanic front of the Mexican Volcanic Belt. *Geofísica Internacional*, 24(1).  
833
- 834 Luhr, J.F., and Prestegard, K.L., 1988. Caldera formation at Volcán Colima, Mexico, by a large  
835 holocene volcanic debris avalanche. *Journal of Volcanology and Geothermal Research*, 35(4), 335-  
836 348.  
837
- 838 Luhr JF., 2002. Petrology and geochemistry of the 1991 and 1998-1999 lava flows from Volcan  
839 Colima, Mexico. *J Volcanol Geotherm Res* 117: 169–194.  
840
- 841 Maccaferri, F., Bonafede, M., and Rivalta, E., 2010. A numerical model of dyke propagation in  
842 layered elastic media. *Geophysical Journal International*, 180(3), 1107-1123.  
843
- 844 Maccaferri, F., Bonafede, M., and Rivalta, E., 2011. A quantitative study of the mechanisms  
845 governing dike propagation, dike arrest and sill formation. *Journal of Volcanology and Geothermal*  
846 *Research*, 208(1-2), 39-50.  
847
- 848 Maccaferri, F., Rivalta, E., Keir, D., and Acocella, V., 2014. Off-rift volcanism in rift zones  
849 determined by crustal unloading. *Nature Geoscience*, 7(4), 297-300.  
850
- 851 Maccaferri, F., Smittarello, D., Pinel, V., and Cayol, V., 2019. On the propagation path of magma-  
852 filled dikes and hydrofractures: The competition between external stress, internal pressure, and crack  
853 length. *Geochemistry, Geophysics, Geosystems*, 20(4), 2064-2081.  
854
- 855 Macías, J.L., Saucedo, R., Gavilanes, J.C., Varley, N., Velasco, García S., Bursik, M.I., Vargas,  
856 Gutiérrez V., Cortés, A., 2006. Flujos piroclásticos asociados a la activi- dad explosiva del Volcán de  
857 Colima y perspectivas futuras. *GEOS* 25(3), 340–351.
- 858 Macías J, Arce J, Sosa G, Gardner JE, Saucedo R., 2017. Storage conditions and magma processes  
859 triggering the 1818CE Plinian eruption of Volcán de Colima. *J Volcanol GeothermRes*  
860 doi:10.1016/j.jvolgeores.2017.02.025.
- 861 Macdonald, K.C., 1982. Mid-ocean ridges: fine scale tectonic, volcanic and hydrothermal pro-  
862 cesses within the plate boundary zone. *Annual Review of Earth and Planetary Sciences* 10, 155–190.
- 863 MacLeod, C.J., Yaouancq, G., 2000. A fossil melt lens in the Oman ophiolite: implications for  
864 magma chamber processes at fast spreading ridges. *Earth and Planetary Science Letters* 176, 357–373.
- 865 Manconi A., Walter TR, and Amelung, F., 2007. Effects of mechanical layering on volcano  
866 deformation. *Geophys. J. Int.* (2007) 170, 952–958.
- 867 Manconi, A., Longpré, M.A., Walter, T.R., Troll, V.R., Hansteen, T.H., 2009. The effects of flank  
868 collapses on volcano plumbing systems. *Geology* 37 (12), 1099–1102.

- 869 Marinos, P. and Hoek, E., 2000. GSI: a geologically friendly tool for rock mass strength estimation.  
870 In: Proc. GeoEng2000 Conference, Melbourne, 1422–1442.
- 871 Martí, J., and Geyer, A., 2009. Central vs flank eruptions at Teide–Pico Viejo twin stratovolcanoes  
872 (Tenerife, Canary Islands). *Journal of Volcanology and Geothermal Research*, 181(1-2), 47-60.  
873
- 874 Massaro S, Sulpizio R, Costa A, Capra L., Lucchi F., 2018. Understanding eruptive style variations at  
875 calc-alkaline volcanoes: the 1913 eruption of Fuego de Colima volcano (Mexico). *Bulletin of*  
876 *Volcanology*, 80:62.
- 877 Massaro, S., Costa, A., Sulpizio, R., Coppola, D., Capra, L., 2019. Cyclic activity of Fuego de  
878 Colima volcano (Mexico): insights from satellite thermal data and non-linear models. *Solid Earth*,  
879 1429-1450.
- 880 Margottini, C., Canuti, P., Sassa, K., 2013. *Landslide science and practice (Vol. 1)*. Berlin: Springer.  
881
- 882 Masterlark, T., Feigl, K.L., Haney, M., Stone, J., Thurber, C., and Ronchin, E., 2012. Nonlinear  
883 estimation of geometric parameters in FEMs of volcano deformation: Integrating tomography models  
884 and geodetic data for Okmok volcano, Alaska. *Journal of Geophysical Research: Solid Earth*,  
885 117(B2).  
886
- 887 Medina-Martínez, F., Espíndola, J.M., De la Fuente, M., Mena, M., 1996. A gravity model of the  
888 Colima, México region. *Geofis. Int.* 35(4), 409–414.
- 889 Michaeli, W., 1991. *Extrusionswerkzeuge für Kunststoffe und Kautschuk: Bauarten, Gestaltung und*  
890 *Berechnungsmöglichkeiten*. Hanser Verlag.  
891
- 892 Moeck, I., Schandelmeier, H. and Holl, H.G., 2009. The stress regime in a Rotliegend reservoir of  
893 the Northeast German Basin. *Int. J. Earth. Sci.* 98, 1643-1654.
- 894 Mutter, J.C., Carbotte, S.M., Su, W.S., Xu, L.Q., Buhl, P., Detrick, R.S., Kent, G.M., Orcutt, J.A.,  
895 Harding, A.J., 1995. Seismic images of active magma systems beneath the East Pacific Rise between  
896 17-degrees-05's and 17-degrees-35's. *Science* 268, 391–395.
- 897 Newman, A. V., Dixon, T. H., Ofoegbu, G. I., and Dixon, J. E., 2001. Geodetic and seismic  
898 constraints on recent activity at Long Valley Caldera, California: evidence for viscoelastic rheology.  
899 *Journal of Volcanology and Geothermal Research*, 105(3), 183-206.  
900
- 901 Norini, G., Agliardi, F., Crosta, G., Groppelli, G., and Zuluaga, M.C., 2019. Structure of the Colima  
902 Volcanic Complex: Origin and Behaviour of Active Fault Systems in the Edifice. In *Volcán de*  
903 *Colima* (pp. 27-54). Springer, Berlin, Heidelberg.  
904
- 905 Norini G, Capra L, Groppelli G, Agliardi F, Pola A, Cortes A., 2010. Structural architecture of the  
906 Colima Volcanic Complex. *J Geophys Res* 115, B12209.  
907
- 908 Núñez-Cornú F, Nava FA, De la Cruz-Reyna S, Jiménez Z, Valencia C, García-Arthur R., 1994.  
909 Seismic activity related to the 1991 eruption of Colima Volcano, Mexico. *Bull Volcanol* 56: 228–237.  
910
- 911 Parfitt, E. A., and L. Wilson, 2008. "The role of volatiles." *Fundamentals of Physical Volcanology*,  
912 64-76.  
913
- 914 Pinel, V., and Jaupart, C., 2004. Magma storage and horizontal dyke injection beneath a volcanic  
915 edifice. *Earth and Planetary Science Letters*, 221(1-4), 245-262.  
916
- 917 Pinel, V., Carrara, A., Maccaferri, F., Rivalta, E., and Corbi, F., 2017. A two-step model for  
918 dynamical dike propagation in two dimensions: Application to the July 2001 Etna eruption. *Journal*  
919 *of Geophysical Research: Solid Earth*, 122(2), 1107-1125.  
920
- 921 Pritchard, M. E., and Simons, M., 2004. An InSAR-based survey of volcanic deformation in the

- 922 central Andes. *Geochemistry, Geophysics, Geosystems*, 5(2).  
 923
- 924 Rao S.S., 1989. *The Finite Element Method in Engineering* second edition. PERGAMON PRESS  
 925 1989 ISBN 0-08-033419-9.
- 926 Rao, S.S., 2013. *The Finite Element Method in Engineering: Pergamon International Library of*  
 927 *Science, Technology, Engineering and Social Studies*. Elsevier.  
 928
- 929 Reubi, O., Blundy, J., and Varley, N.R., 2013. Volatiles contents, degassing and crystallisation of  
 930 intermediate magmas at Volcan de Colima, Mexico, inferred from melt inclusions. *Contributions to*  
 931 *Mineralogy and Petrology*, 165(6), 1087-1106.  
 932
- 933 Reubi, O., Blundy, J., and Pickles, J., 2019. Petrological monitoring of Volcán de Colima magmatic  
 934 system: the 1998 to 2011 activity. In *Volcán de Colima* (pp. 219-240). Springer, Berlin, Heidelberg.  
 935 Rivalta et al., 2019. Stress inversions to forecast magma pathways and eruptive vent location *Sci.*  
 936 *Adv.* 2019; 5:eaa9784 .
- 937 Rivalta, E., Corbi, F., Passarelli, L., Acocella, V., Davis, T., and Di Vito, M.A., 2019. Stress  
 938 inversions to forecast magma pathways and eruptive vent location. *Science advances*, 5(7), eaa9784.  
 939
- 940 Robin, C., Mossand, P., Camus, G., Cantagrel, J. M., Gourgaud, A., and Vincent, P.M., 1987.  
 941 Eruptive history of the Colima volcanic complex (Mexico). *Journal of Volcanology and Geothermal*  
 942 *Research*, 31(1-2), 99-113.  
 943
- 944 Ronchin, E., Masterlark, T., Molist, J. M., Saunders, S., and Tao, W., 2013. Solid modeling  
 945 techniques to build 3D finite element models of volcanic systems: an example from the Rabaul  
 946 Caldera system, Papua New Guinea. *Computers & Geosciences*, 52, 325-333.  
 947
- 948 Ronchin, E., Geyer, A., and Martí, J., 2015. Evaluating topographic effects on ground deformation:  
 949 insights from finite element modeling. *Surveys in Geophysics*, 36(4), 513-548.  
 950
- 951 Rosas-Elguera, J., Ferrari, L., Garduño-Monroy, V.H., Urrutia-Fucugauchi, J., 1996: Continental  
 952 boundaries of the Jalisco block and their influence in the Pliocene-Quaternary kinematics of western  
 953 Mexico. *Geology* 24, 921-924.
- 954 Rosas-Elguera J, Ferrari L, Martinez ML, Urrutia-Fucugauchi J., 1997. Stratigraphy and tectonics of  
 955 the Guadalajara region and triple- junction area, western Mexico. *Int Geol Rev* 39:125-140.  
 956 doi:10.1080/00206819709465263.
- 957 Rosas-Elguera, J., Alva-Valdivia, L. M., Goguitchaichvili, A., Urrutia-Fucugauchi, J., Ortega-Rivera,  
 958 M. A., Prieto, J.C.S., and Lee, J.K., 2003. Counterclockwise rotation of the Michoacan Block:  
 959 implications for the tectonics of western Mexico. *International Geology Review*, 45(9), 814-826.  
 960
- 961 Roverato, M., Capra, L., Sulpizio, R., Norini, G., 2011. Stratigraphic reconstruction of two debris  
 962 avalanche deposits at Colima Volcano (Mexico): insights into pre-failure conditions and climate  
 963 influence. *Journal of Volcanology and Geothermal Research*, 207(1-2), 33-46, 2011
- 964 Roverato, M., and Capra, L., 2013. Características microtexturales como indicadores del transporte y  
 965 emplazamiento de dos depósitos de avalancha de escombros del Volcán de Colima (México). *Revista*  
 966 *mexicana de ciencias geológicas*, 30(3), 512-525.  
 967
- 968 Salzer J.T., Nikkhoo M., Walter T., Sudhaus H., Reyes-Dávila G., Bretòn-Gonzalez M., Aràmbula R.,  
 969 2014. Satellite radar data reveal short-term pre-explosive displacements and a complex conduit  
 970 system at Volcan de Colima, Mexico. *Front Earth Sci* 2:12.  
 971
- 972 Saada, A.S., 2009. *Elasticity: Theory and Applications*. Krieger, Malabar, Florida.
- 973 Savin, G. N., 1961. Stress concentration around holes.  
 974

- 975 Saucedo R, Macías J., Gavilanes JC, Arce JL, Komorowski JC, Gardner JE, Valdez-Moreno G., 2010.  
 976 Eyewitness, stratigraphy, chemistry, and eruptive dynamics of the 1913 Plinian eruption of Volcán  
 977 de Colima. México. *J Volcanol Geotherm Res* 191:149–166.  
 978
- 979 Saucedo R, Macías JL, Gavilanes JC, Arce JL, Komorowski JC, Gardner JE, and Valdez-Moreno G.,  
 980 2011. Corrigendum to Eyewitness, stratigraphy, chemistry, and eruptive dynamics of the 1913 plinian  
 981 eruption of Volcan de Colima, Mexico. *J Volcanol Geotherm Res* 191:149–166.  
 982
- 983 Schwarz, H.R., 1991. *Methode der finiten Elemente neubearbeitete Auflage*, B.G. Teubner Stuttgart  
 984 ISBN 3-519-22349-X.
- 985 Selvans, M. M., Stock, J. M., DeMets, C., Sanchez, O., and Marquez-Azua, B., 2011. Constraints on  
 986 Jalisco Block motion and tectonics of the Guadalajara triple junction from 1998–2001 Campaign  
 987 GPS Data. *Pure and applied geophysics*, 168(8-9), 1435-1447.  
 988
- 989 Serpa, L., Smith, S., Katz, C., Skidmore, C., Sloan, R., Pavlis, T., 1992. A geophysical investigation  
 990 of the southern Jalisco block in the state of Colima, Mexico. *Geofisica Internacional* 31, 247–252.
- 991 Simms MA., and Graven G., 2004. Thermal convection in faulted extensional sedimentary basins:  
 992 theoretical results from finite-element modelling. *Geofluids* (2004), 4, 109-130.  
 993
- 994 Singh, S. C., Crawford, W. C., Carton, H., Seher, T., Combiér, V., Cannat, M., and Miranda, J. M.,  
 995 2006. Discovery of a magma chamber and faults beneath a Mid-Atlantic Ridge hydrothermal field.  
 996 *Nature*, 442(7106), 1029.  
 997
- 998 Sinton, J.M., and Detrick, R.S., 1992. Mid-ocean ridge magma chambers. *Journal of Geophysical*  
 999 *Research: Solid Earth*, 97(B1), 197-216.  
 L000
- L001 Stock JM and Lee J., 1994. Do microplates in subduction zones leave a geological record? *Tectonics*  
 L002 13:1472–1487.
- L003 Stoores, G. R., and Sheridan, M.F., 1992. Giant debris avalanches from the Colima Volcanic  
 L004 Complex, Mexico: Implications for long-runout landslides (> 100 km) and hazard assessment.  
 L005 *Geology*, 20(4), 299-302.  
 L006
- L007 Spica, Z., Cruz-Atienza, V.M., Reyes-Alfaro, G., Legrand, D., and Iglesias, A., 2014. Crustal  
 L008 imaging of western Michoacán and the Jalisco Block, Mexico, from ambient seismic noise. *Journal*  
 L009 *of Volcanology and Geothermal Research*, 289, 193-201.  
 L010
- L011 Spica Z, Perton M, Legrand D., 2017. Anatomy of the Colima volcano magmatic system,  
 L012 Mexico, *Earth Planet Sci Lett* 459: 1-13.  
 L013
- L014 Suárez, G., Garcia-Acosta, V., Gaulon, R., 1994. Active crustal deformation in the Jalisco block,  
 L015 Mexico: evidence for a great historical earthquake in the 16th century. *Tectonophysics* 234, 117–12.
- L016 Sulpizio, R., Lucchi, F., Forni, F., Massaro, S., and Tranne, C., 2016. Unravelling the effusive-  
 L017 explosive transitions and the construction of a volcanic cone from geological data: The example of  
 L018 Monte dei Porri, Salina Island (Italy). *Journal of Volcanology and Geothermal Research*, 327, 1-22.  
 L019
- L020 Sulpizio, R., and Massaro, S., 2017. Influence of stress field changes on eruption initiation and  
 L021 dynamics: a review. *Frontiers in Earth Science*, 5, 18.  
 L022
- L023 Tibaldi, A., 2015. Structure of volcano plumbing systems: A review of multi-parametric effects.  
 L024 *Journal of Volcanology and Geothermal Research* 298 (2015) 85–135.
- L025 Touloukian, Y.S., Judd, W.R., Roy, R.F., 1989. *Physical Properties of Rocks and Minerals*, vol. 548.  
 L026 Hemisphere, New York.
- L027 Turcotte, D. L. and Schubert, G., 2002. *Geodynamics*, 2nd edition, Cambridge University Press.

L028 Zehner B, Jana H. Börner J.H., Görz I., Spitzer K., 2015. Workflows for generating tetrahedral  
L029 meshes for finite element simulations on complex geological structures. Computers and Geosciences,  
L030 79, 105-117.

L031 Zhao, S., Muller, R. D., Takahashi, Y. and Kaneda, Y., 2004. 3-D finite-element modelling of  
L032 deformation and stress associated with faulting: effect of inhomogeneous crustal structures, Geophys.  
L033 J. Int., 157, 629– 644.

L034 Zhong, X. Marcin, Dabrowski, Bjørn Jamtveit, 2019. Analytical solution for the stress field in elastic  
L035 half space with a spherical pressurized cavity or inclusion containing eigenstrain. Geophysical  
L036 Journal International · (submitted).

L037 Zobin, V.M., Luhr, J.F., Taran, Y.A., Bretón, M., Cortés,A., De la Cruz-Reyna, S., Domínguez, T.,  
L038 Galindo, I., Gavilanes, J.C., Muñiz, J.J., Navarro, C., Ramírez, J. J., Reyes, G.A., Ursúa, M., Velasco,  
L039 J., Alatorre, E., Santiago, H., 2002. Overview of the 1997–2000 activity of Volcán de Colima,  
L040 Mexico. J. Volcanol. Geotherm.Res. 117, 1–19.

L041 Watanabe, T., Masuyama, T., Nagaoka, K., Tahara, T., 2002. Analog experiments on magma-filled  
L042 cracks: competition between external stresses and internal pressure. Earth Planets Space 54, 1247–  
L043 1261.

L045 Wang, R., Martin, F.L. and Roth, F., 2003. Computation of deformation induced by earthquakes in a  
L046 multi-layered elastic crust-FORTRAN programs EDGRN/EDCMP, Comput. Geosci., 29, 195–207.  
L047

L048 **Table 1 - [Element types used in LISA analysis considering the final conduit feeding system](#)**  
L049 **[configuration – Fig.1d, panel vi\)](#)**

<i>E-W cross-section (a-a')</i>		Element Type	Elements	Nodes
FC	Fuego de Colima	quad4-tri3	372	384
VD	Volcanic Deposits	quad4-tri3	245	273
GF	Graben Fill	quad4-tri3	456	338
B	Basament	quad4-tri3	3088	2907
CG	Colima graben	quad4-tri3	48	71
<u>Total Elements: 4209</u>				

L057 **Table 2 - Rock mass and mechanical properties [of the geological Units](#)** used in the finite-element  
L058 model (from Norini et al., 2010, 2019).  
L059

Acronym	Model Unit	Rock Type	Density (kg/m <sup>3</sup> )	Young's Modulus (MPa)	Poisson's ratio $\nu$
FC	Fuego de Colima	Andesitic lavas and pyroclastic deposits forming the Paleofuego-Fuego de Colima	2242	$1.4 \times 10^3$	0.30

		volcano			
VD	Volcaniclastic deposits	Pyroclastic and epiclastic deposits covering the southern flank of the CVC	1539	$1.7 \times 10^3$	0.32
GF	Graben Fill	Quaternary alluvial, colluvial, lacustrine deposits filling the graben	1834	$1.5 \times 10^3$	0.35
B	Basement	Cretaceous limestones and intrusive rocks forming the bed-rock underlying the CVC	2650	$3.6 \times 10^4$	0.30

L060

L061

## L062 Figures Captions

L063

L064 **Fig. 1** (a) Morphotectonic map of the Colima Volcanic Complex (NC=Nevado de Colima volcano;  
L065 FC=Fuego de Colima volcano) and Colima Rift with the main tectonic and volcano-tectonic  
L066 structures (NCG =Northen Colima Graben; CCG= Central Colima Graben, from Norini et al., 2019).  
L067 In the inset, the location of the Colima Volcanic Complex (CVC) within the Trans-Mexican Volcanic  
L068 Belt (TMVB) is shown in the frame of the subduction-type geodynamic setting of Central America  
L069 (from Davila et al., 2019); (b) general sketch of the geometrical configurations used in [LISA](#); (c)  
L070 [example of mesh of the investigated area for the dual magma chamber model with conduits \(case v in](#)  
L071 [panel \(b\), considering zero-displacement along the bottom and left and right sides. Note that for case](#)  
L072 [\(vi\) in panel \(b\) the zero-displacement is removed from the lateral sides; \(d\) sketch of the Fuego de](#)  
L073 [Colima feeding system composed of a 15 km-deep magma chamber connected to surface via a 6 km-](#)  
L074 [deep magma chamber and dykes.  \$\Delta P\_{chs}\$  and  \$\Delta P\_{chd}\$  are the magmatic overpressures in the shallow](#)  
L075 [and deep chambers, respectively \(modified from Massaro et al., 2019\).](#)

L076

L077 **Fig. 2** [Results of the sensitivity analysis carried out on](#) the Young's Modulus variations within [each](#)  
L078 [rock layer of the domain considering different configurations \(stratified substratum model – nodes:](#)  
L079 [4426; single magma chamber model – nodes: 4426; dual magma chamber model – nodes: 4161; dual](#)  
L080 [magma chamber with conduits model – nodes: 3737\). For each geological Unit \(B, FC, GF, VD\), the](#)  
L081 [relative global variation in  \$L\_2\$  \(%\) is provided for  \$\sigma\_1\$  and  \$\sigma\_3\$ . The  \$x\(-\)\$  and  \$x\(+\)\$  vectors indicate the](#)  
L082 [Young's Modulus variation by an order of magnitude with respect to  \$x\_{ref}\$  vector, containing the stress](#)  
L083 [values calculated by using the values of material's properties indicated in Table 2.](#)

L084

L085 **Fig. 3** Spatial variation (%) of the  $L_2$  norm's components at varying Young's Modulus [for selected](#)  
L086 [cases of Units B and VD: \(a\) Unit B in the stratified substratum model \(nodes: 4426\); \(b\) Unit B in](#)  
L087 [the single magma chamber model \(nodes: 4426\); \(c\) Unit B in the dual magma chamber model](#)

L088 [\(nodes: 4161\); \(d\) Unit VD in the dual magma chamber with conduits model \(nodes: 3737\). Symbols](#)  
L089 [x\(-\) and x\(+\) have the same meaning of Figure 2.](#)

L090  
L091 **Fig. 4** E-W gravitational modelling of the CVC domain. The scale of the mesh is expressed in Unit  
L092 of Design (1 UD = 1 km). The domain extends 60 km along the  $x$ -axis, and 30 km along the  $z$ -axis.  
L093 [The number of nodes used in the mesh is set to 4426.](#) The magnitude and pattern of the principal  
L094 stresses (dotted black lines) are reported for (a) [the homogeneous stratigraphy](#) (Unit FC = andesitic  
L095 lavas and pyroclastic deposits) and for (b) [the not homogeneous stratigraphy](#) (Unit FC; Unit B =  
L096 Cretaceous limestones and intrusive rocks forming the bed-rock underlying the CVC; Unit GF =  
L097 Quaternary alluvial, colluvial, and lacustrine deposits filling the graben; Unit VD = volcanoclastic  
L098 deposits covering the southern flank of the CVC). The blue [line contours](#) the unperturbed part of the  
L099 domain, which extends ca. 30 km horizontally and ca. [25 km](#) vertically. [Note that the scale of stress](#)  
L100 [values is the same for the all simulations.](#)

L101  
L102  
L103 **Fig. 5** E-W gravitational modelling of the CVC domain [with a not homogeneous stratigraphy](#). The  
L104 magnitude and pattern of the principal stresses are reported for (a) the single magma chamber model  
L105 represented by a magma chamber ( $2a = 14$  km and  $2b = 3.6$  km) at 15 km of depth, [and \(b\) the dual](#)  
L106 [magma chamber model composed of a 15 km-deep magma chamber \( \$2a = 14\$  km and  \$2b = 3.6\$  km\)](#)  
L107 [and a shallow 6 km-deep one \( \$2a = 3.5\$  km and  \$2b = 2\$  km\).](#) The magma chambers are not connected.  
L108 [The magmatic overpressures are set to 10 and 5 MPa for the 15 km-deep and 6 km-deep magma](#)  
L109 [chambers, respectively. The number of nodes is set to 4426 and 4161 for the single and dual magma](#)  
L110 [chamber models, respectively. Black dotted lines highlight the passage from different stress values.](#)  
L111 [The red dotted line in panel \(b-i\) indicates the formation of the stress arch. Note that the scale of](#)  
L112 [stress values are different for each panel in order to maximise the simulation details.](#)

L113  
L114 **Fig. 6** E-W gravitational modelling of the CVC domain [with a not homogeneous stratigraphy](#)  
L115 [accounted](#) for a dual magma chamber system connected by dykes via surface (deep magma chamber,  
L116  $2a = 14$  km and  $2b = 3.6$  km at 15 km of depth; shallow magma chamber,  $2a = 3.5$  km and  $2b = 2$  km  
L117 at 6 km [od depth](#)). [The magnitude and pattern of the principal stresses are shown. The number of](#)  
L118 [nodes used is set to 3737. The magmatic overpressures are set to 10 and 5 MPa for the 15 km-deep](#)  
L119 [and 6 km-deep magma chambers, respectively. The black dotted lines in panel \(ii\) highlight the](#)  
L120 [passage from different stress values. Note that the scale of stress values are different for each panel in](#)  
L121 [order to maximise the simulation details.](#)

L122  
L123 **Fig. 7** E-W gravitational modelling of the CVC domain [with a not homogeneous stratigraphy](#)

L124 considering [the extensional field stress](#). The magnitude and pattern of the principal stresses are shown  
L125 for the single magma chamber model ([panels i-ii](#)), the dual magma chamber model ([panels iii-iv](#)), the  
L126 dual magma chamber with conduits model ([panels v-vi-vii-viii](#)). [Note that in panel vii-viii the faults](#)  
L127 [bordering the Colima graben are shown. For all configurations an extensive far-field stress of 5 MPa](#)  
L128 [is applied at the lateral boundaries of the domain. In panels vii-viii the additional effect of the local](#)  
L129 [extensive field is simulated using a reduced values of material's properties \(Table 2\). The magmatic](#)  
L130 [overpressures are set to 10 and 5 MPa for the 15 km-deep and 6 km-deep magma chambers,](#)  
L131 [respectively. Black dotted lines highlight the passage from different stress values. The red arrows](#)  
L132 [indicate the direction of the applied far field stress. Note that the scale of stress values are different](#)  
L133 [for each panel in order to maximise the simulation details.](#)

L134

L135

L136

L137

L138

L139

L140

L141

L142

## [Figures](#)

L143

L144

L145

L146

L147

L148

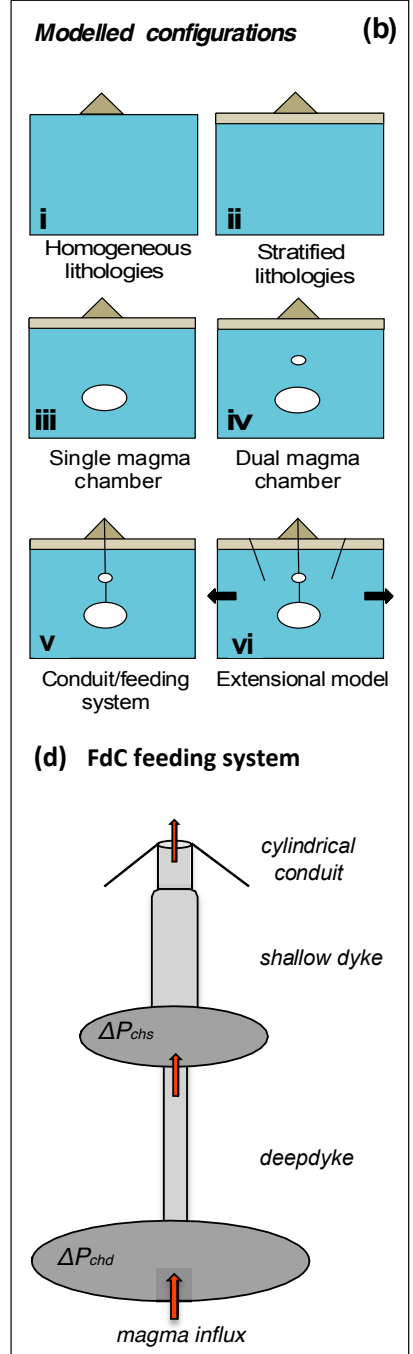
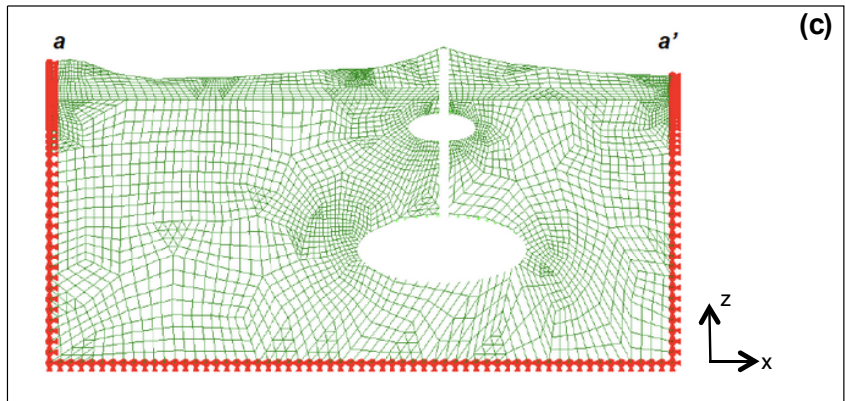
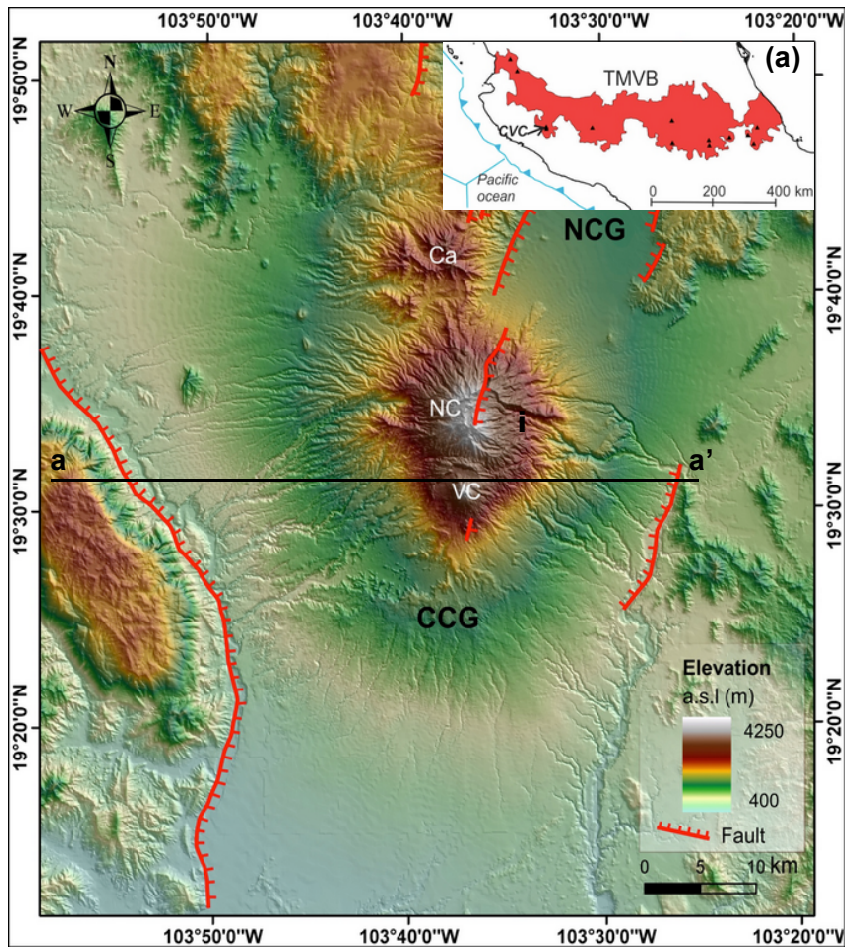
L149

L150

L151

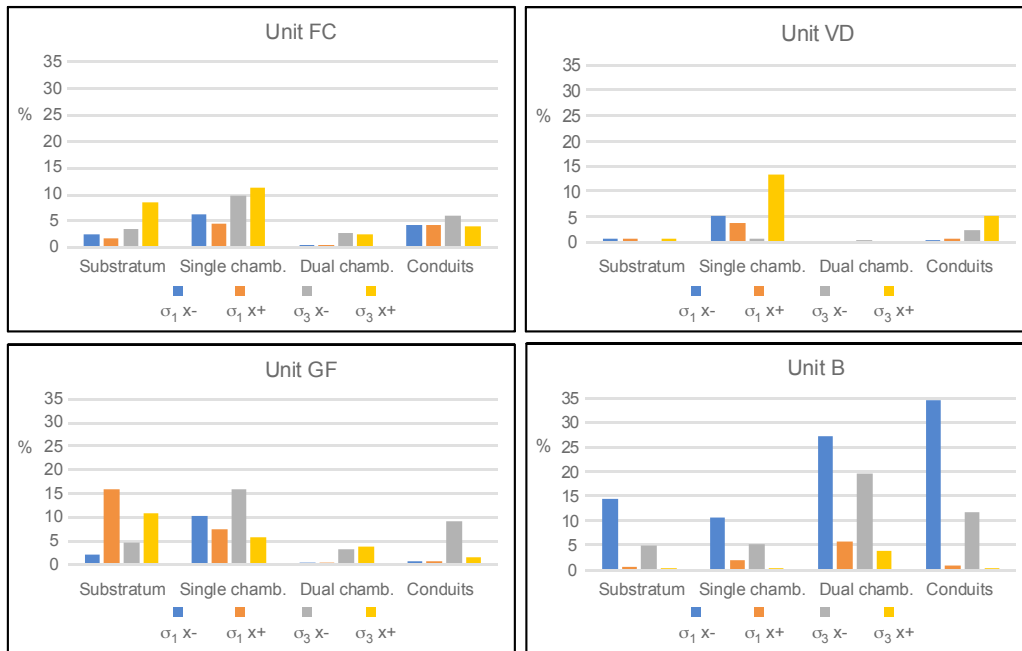


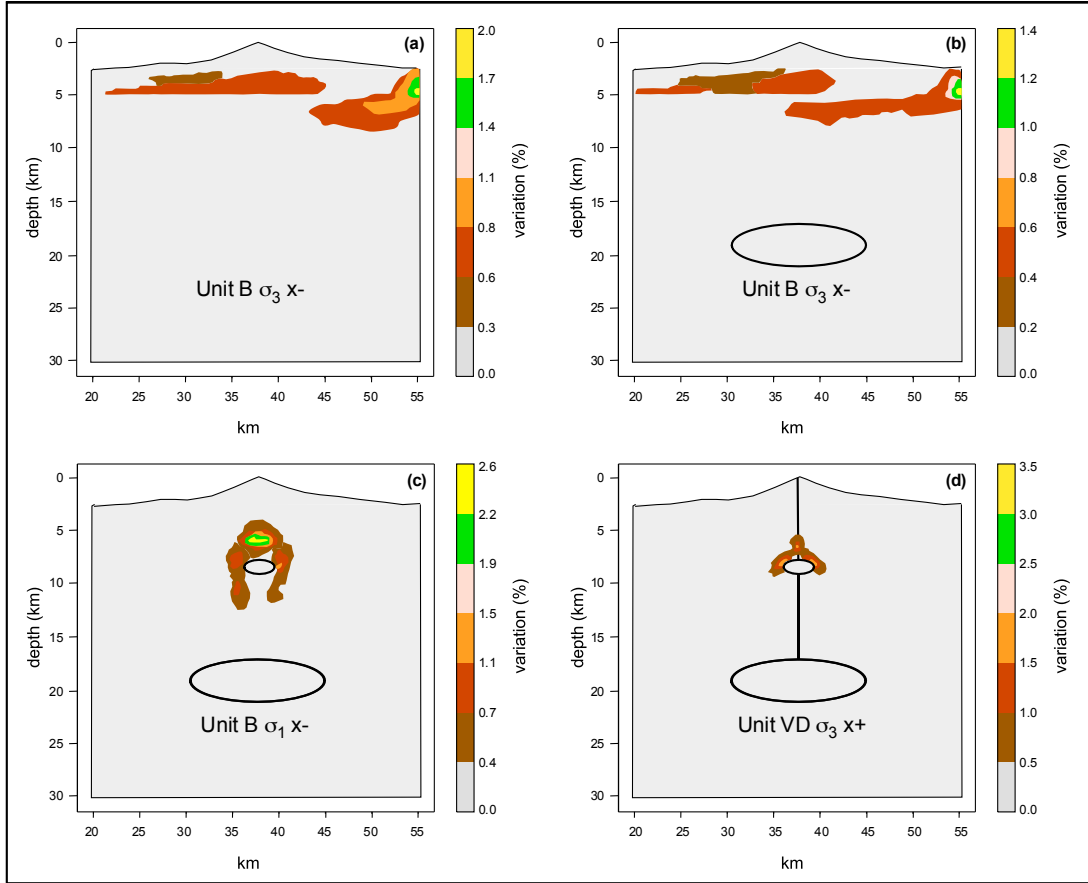
L152 Figure 1

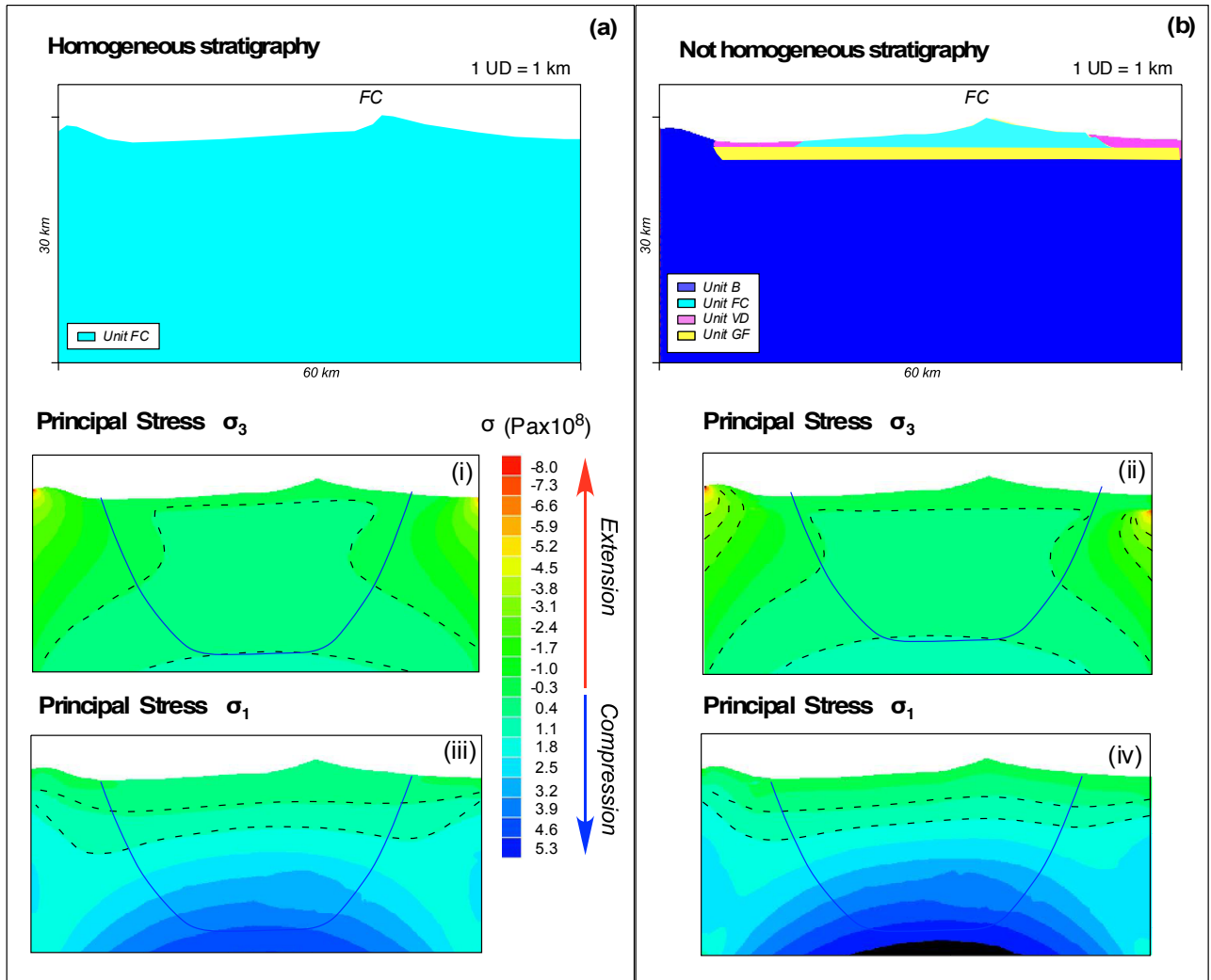


L153

L154





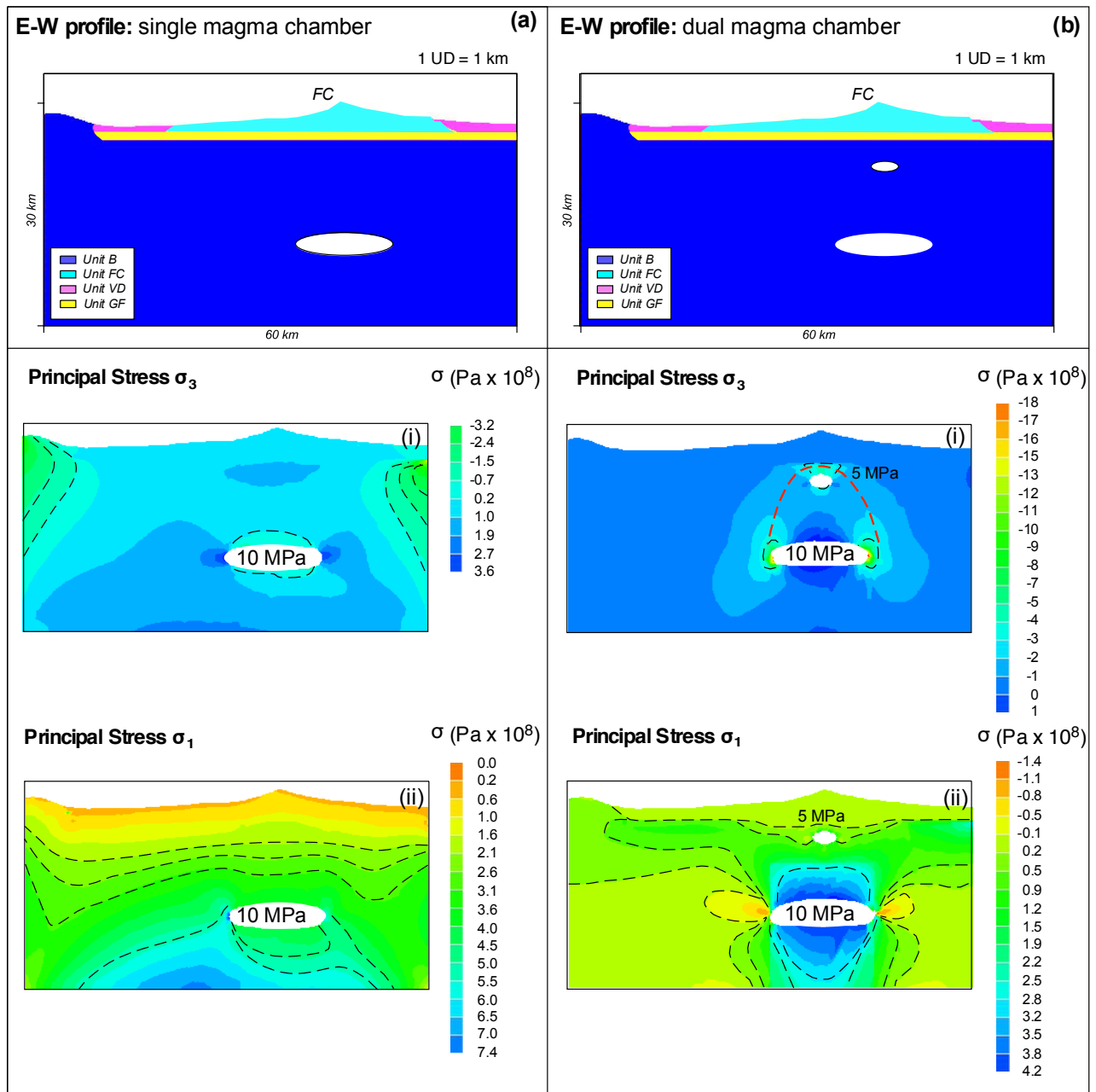


L162

L163

L164

L165



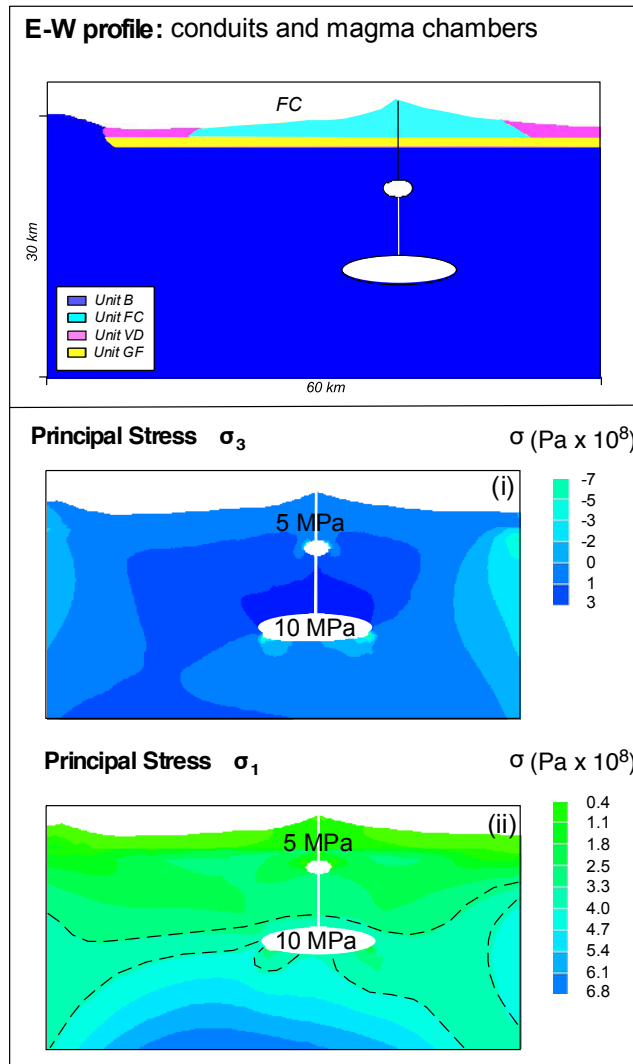
L167

L168

L169

L170

L171 [Figure 6](#)

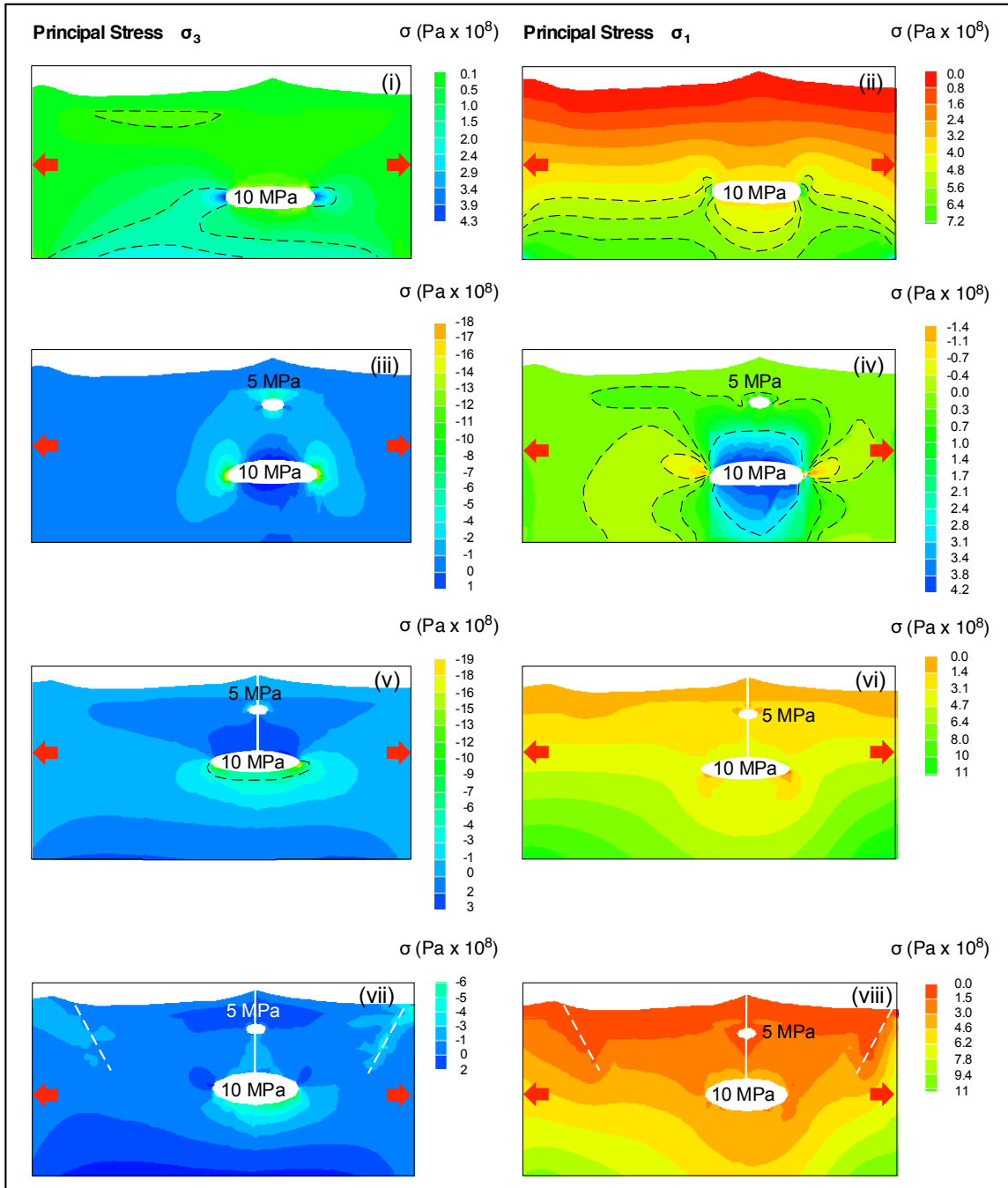


L172

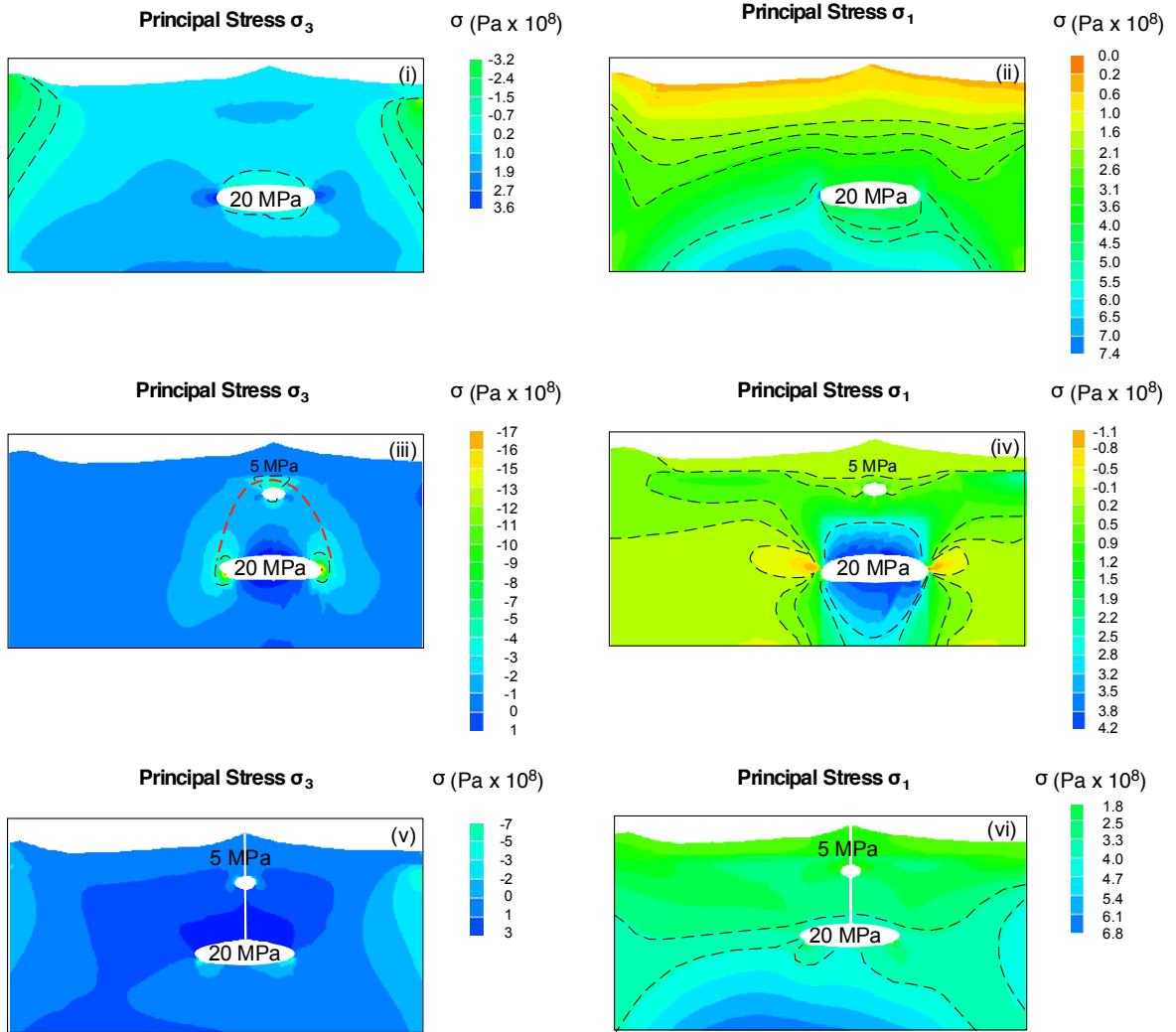
L173

L174

L175



Appendix 1





Appendix 2

